

Self-interaction corrected relativistic theory of magnetic scattering of x rays: Application to praseodymium

M. Horne,¹ E. Arola,^{1,2} P. Strange,¹ H. Winter,³ Z. Szotek,⁴ and W.M. Temmerman⁴

¹*School of Chemistry and Physics, Keele University, Staffordshire ST5 5BG, United Kingdom*

²*Optoelectronics Research Centre, Tampere University of Technology, P.O. Box 692, FIN-33101 Tampere, Finland*

³*INFP, Forschungszentrum Karlsruhe GmbH, Postfach 3640, D-76021 Karlsruhe, Germany* and

⁴*Daresbury Laboratory, Daresbury, Warrington, WA4 4AD, Cheshire, United Kingdom*

(Dated: February 20, 2019)

Resonant magnetic scattering spectra of x-rays from elemental praseodymium with the face-centered cubic crystal structure are computed and analyzed. The scattering amplitudes are calculated using a standard time-dependent perturbation theory to second order in the electron-photon interaction vertex. In order to calculate the cross section reliably an accurate description of the electronic states in the material under investigation is required and this is provided by the density functional theory (DFT) employing the Local Spin Density Approximation combined with the self-interaction corrections (SIC-LSD). The magnetic x-ray resonant scattering (MXRS) theory has been implemented in the framework of the relativistic spin-polarized LMTO-ASA band structure calculation method. It is shown that the theory quantitatively reproduces the dependence on the spin and orbital magnetic moments originally predicted qualitatively (Blume, *J. Appl. Phys.*, **57**, 3615, (1985)) and yields results that can be compared directly with experiment.

PACS numbers: PACS numbers: 78.70.Ck, 75.25.+z, 71.15.-m, 71.20.Eh

I. INTRODUCTION

Magnetic X-Ray Scattering (MXRS) is a well-developed technique for probing the magnetic and electronic structure of materials. The foundations of the theory of MXRS were laid down by Blume¹. Later on Blume and Gibbs² developed the theory further to show that the orbital and spin contributions to the magnetic moment can be measured separately using MXRS with a judicious choice of experimental geometry and polarization of the x-rays. Hannon *et al.*³ presented a nonrelativistic theory of x-ray resonance exchange scattering and wrote down explicit expressions for the electric dipole ($E1$) and quadrupole ($E2$) contributions. This work is based on an atomic model of magnetism and has been applied successfully to a variety of materials including UAs and Gd by Fasolino *et al.*⁴. Rennert⁵ produced a semi-relativistic theory of MXRS written in terms of Green's functions, but no such calculations have been performed. More recently, theory based on an atomic model of the electronic structure of materials has been written down by Lovesey⁶ and co-workers and applied successfully to a variety of materials. A first-principles theory of MXRS based on a time-dependent second order perturbation theory and density functional theory^{7,8} was produced by Arola *et al.*^{9,10} and applied successfully to several transition metal materials¹¹. This theory is restricted in its range of application because of the limitations imposed by the local density approximation to DFT which means that the theory can only be applied to simple and transition metal materials. This is particularly unfortunate because it is in the rare earth and actinide materials that the most exotic magnetism in the periodic table occurs.

In recent years advances in electronic structure calculations beyond the local density approximation have broadened the range of materials for which numerically accurate electronic structure calculations can be performed. In particular the LDA+U method¹² and the self-interaction corrected local spin density approximation to density functional theory^{13,14,15} have met with considerable success in describing materials with localized electrons. The latter method reduces the degeneracy of the f states at the Fermi level and hence also circumvents all the convergence problems associated with the LSD approximation to DFT in electronic structure calculations for rare earth materials. Notably, the SIC-LSD has provided a very good description of the rare earth metal and rare earth chalcogenide crystal structures.¹⁶ A relativistic version of the SIC formalism has been derived¹⁷ that has been shown to yield an excellent description of the electronic structure of rare earth materials in the few cases to which it has been applied. This method is reviewed by Temmerman *et al.*¹⁴

The fact that electromagnetic radiation can be scattered from the magnetic moments of spin-1/2 particles was first shown by Low, and by Gell-Mann and Goldberger half a century ago.¹⁸ Later on it was Platzman and Tzoar¹⁹ who first proposed the use of x-ray scattering techniques to study the magnetization density of solids. At that time progress in studying magnetic structures using x-rays was severely hampered because the cross section for magnetic scattering is smaller than the cross section for charge scattering¹ by a factor of $(\hbar\omega/mc^2)^2$. It was Gibbs *et al.*²⁰ who first observed a large resonant enhancement of the cross section when the energy of the x-ray is tuned through an absorption edge. Since that time technological advances have produced high resolution, high intensity synchrotron radiation sources that have transformed magnetic x-ray resonant scattering into a practical tool for investigating magnetic and

electronic structures of materials. Nowadays the world's leading synchrotron facilities have beamlines dedicated to this technique²¹ and applications of resonant x-ray scattering are burgeoning. Reviews of the experimental state-of-the-art MXRS techniques have been written by Stirling²² and Cooper²³.

We have recently implemented a first-principles theory of MXRS that is based on a standard time-dependent perturbation theory where the scattering amplitudes are calculated to second order in the electron-photon interaction vertex. To describe MXRS from a given material it is necessary to have an accurate description of the electronic structure of the material in question. This is provided by using the SIC within the LSD approximation to the density functional theory which is implemented using the relativistic spin-polarized LMTO-ASA band structure calculation method²⁴. The theory of MXRS is equivalent to that of Arola *et al.*⁹, but has been rewritten in a form that is appropriate for implementation in connection with the LMTO-ASA method where there is substantial experience of SIC methods. The major step forward reported in this paper is the integration of the SIC into the MXRS theory which enables us to describe rare earth and actinide materials on an equal footing with transition and simple materials.

In this paper, we give a brief description of the MXRS theory and illustrate it in a calculation for praseodymium. The results are analysed and discussed. Finally we show that the present work is consistent with the earlier theory and demonstrate how the MXRS cross section reflects the properties of these materials.

II. THEORY

A. The Relativistic SIC-LSD formalism

The SIC-LSD approximation^{25,26} is an *ab-initio* electronic structure scheme, that is capable of describing localization phenomena in solids.^{14,15,27} In this scheme the spurious self-interaction of each occupied electron state is subtracted from the conventional LSD approximation to the total energy functional, which leads to a greatly improved description of static Coulomb correlation effects over the LSD approximation. This has been demonstrated in studies of the Hubbard model,^{28,29} in applications to 3d monoxides^{15,27} and cuprates,^{13,30,31} *f*-electron systems,^{16,32,33} orbital ordering,³⁴ metal-insulator transitions³¹ and solid hydrogen.³⁵

For many applications it is necessary to account for all relativistic effects including spin-orbit coupling in an electronic structure calculation. Relativistic effects become progressively more important as we proceed to heavier elements. They are also extremely important when we are considering properties dependent on orbital moments and their coupling to electron spins.

The relativistic total energy functional in the local spin density approximation is

$$E^{LSD}[\bar{n}(\mathbf{r})] = E_{kin}[n(\mathbf{r})] + U[n(\mathbf{r})] + \int V^{\text{ext}}(\mathbf{r})n(\mathbf{r})d\mathbf{r} + E_{xc}^{LSD}[\bar{n}(\mathbf{r})] - \int B^{\text{ext}}(\mathbf{r})m(\mathbf{r})d\mathbf{r} \quad (1)$$

where $\bar{n}(\mathbf{r}) = (n^{\uparrow}(\mathbf{r}), n^{\downarrow}(\mathbf{r})) (\equiv (n(\mathbf{r}), m(\mathbf{r})))$ labels the spin up and spin down charge density.

$$E_{kin}[n(\mathbf{r})] = \sum_{\Lambda} \langle \psi_{\Lambda} | \hat{T} | \psi_{\Lambda} \rangle \quad (2)$$

$$E_{xc}^{LSD}[\bar{n}(\mathbf{r})] = \int n(\mathbf{r}) \epsilon_{xc}[\bar{n}(\mathbf{r})] d\mathbf{r} \quad (3)$$

Here \hat{T} is an operator describing the kinetic energy and rest mass of the electrons

$$\hat{T} = \frac{c\hbar}{i} \alpha \cdot \nabla + mc^2(\beta - I) \quad (4)$$

where α and β are the usual relativistic matrices³⁶. $U[n(\mathbf{r})]$ represents all two particle interactions including the Breit interaction. $V^{\text{ext}}(\mathbf{r})$ is the external potential, $B^{\text{ext}}(\mathbf{r})$ is an external magnetic field. The density $n(\mathbf{r})$ and the spin density $m(\mathbf{r})$ are given by

$$n(\mathbf{r}) = \sum_{\Lambda} \psi_{\Lambda}^{\dagger}(\mathbf{r}) \psi_{\Lambda}(\mathbf{r}) \quad (5)$$

$$m(\mathbf{r}) = \mu_B \sum_{\Lambda} \psi_{\Lambda}^{\dagger}(\mathbf{r}) \sigma \psi_{\Lambda}(\mathbf{r}) \quad (6)$$

where σ is the spin operator and Λ represents the quantum numbers. In Eqs. (6) and (7) below we have implied a representation in which spin is a good quantum number and the sums are over the occupied states. $\epsilon_{xc}[\bar{n}(\mathbf{r})]$ is the exchange correlation energy of a gas of constant density and Eq. (3) is the local spin density approximation.

If we minimise the functional (1) with respect to changes in the density and spin density we obtain a Dirac-like equation:

$$\left(\frac{c\hbar}{i} \alpha \cdot \nabla + mc^2(\beta - I) + V^{eff}(\mathbf{r}) - \mu_B \beta \sigma \cdot \mathbf{B}^{eff}(\mathbf{r}) \right) \psi_\Lambda(\mathbf{r}) = \epsilon_\Lambda \psi_\Lambda(\mathbf{r}) \quad (7)$$

where

$$V^{eff}(\mathbf{r}) = V^{ext}(\mathbf{r}) + \int \int \frac{n(\mathbf{r})n(\mathbf{r}')}{|\mathbf{r} - \mathbf{r}'|} d\mathbf{r} d\mathbf{r}' + \frac{\delta E_{xc}^{LSD}[\bar{n}(\mathbf{r})]}{\delta n(\mathbf{r})} \quad (8)$$

$$B^{eff}(\mathbf{r}) = B^{ext}(\mathbf{r}) + \frac{\delta E_{xc}^{LSD}[\bar{n}(\mathbf{r})]}{\delta m(\mathbf{r})} \quad (9)$$

The Local Spin Density Approximation discussed above provides a very successful description of a variety of properties of condensed matter, but suffers from a drawback because it contains self-interactions of the single particle charges. In an exact theory these spurious self-interactions would precisely cancel. In the LSD the cancellation is only approximate and in materials where there are well-localised electrons this can lead to significant errors. The SIC-LSD approach to this problem is to augment the LSD functional with an extra term that removes this deficiency.

$$E^{SIC-LSD} = E^{LSD} + E^{SIC} \quad (10)$$

where

$$E^{SIC}[\{\bar{n}_\alpha(\mathbf{r})\}] = - \sum_\alpha (U[n_\alpha(\mathbf{r})] + E_{xc}^{LSD}[\bar{n}_\alpha(\mathbf{r})]) \quad (11)$$

where $\bar{n}_\alpha(\mathbf{r}) = (n_\alpha^\uparrow(\mathbf{r}), n_\alpha^\downarrow(\mathbf{r})) (\equiv (n_\alpha(\mathbf{r}), m_\alpha(\mathbf{r}))$ and

$$U[n_\alpha(\mathbf{r})] = \int \frac{n_\alpha(\mathbf{r})n_\alpha(\mathbf{r}')}{|\mathbf{r} - \mathbf{r}'|} d\mathbf{r}' d\mathbf{r} \quad (12)$$

$$E_{xc}^{LSD}[\bar{n}_\alpha(\mathbf{r})] = \int n_\alpha(\mathbf{r}) \epsilon_{xc}[\bar{n}_\alpha(\mathbf{r})] d\mathbf{r} \quad (13)$$

where α runs over all orbitals that are SI-corrected. For the exchange-correlation term in the SIC energy we need to consider a fully spin-polarised electron. The corresponding single particle-like wave equation is obtained by taking the functional derivative of $E^{SIC-LSD}$ with respect to $\psi_\alpha(\mathbf{r})$ and we obtain

$$\left(\frac{c\hbar}{i} \alpha \cdot \nabla + mc^2(\beta - I) + V^{eff}(\mathbf{r}) - \mu_B \beta \sigma \cdot \mathbf{B}^{eff}(\mathbf{r}) + w_\alpha^{SIC}(\mathbf{r}) \right) \psi_\alpha(\mathbf{r}) = \sum_{\alpha'} \lambda_{\alpha,\alpha'} \psi_{\alpha'}(\mathbf{r}) \quad (14)$$

where the SIC potential is given by

$$w_\alpha^{SIC}(\mathbf{r}) = - \left(\int \frac{2n_\alpha(\mathbf{r}')}{|\mathbf{r} - \mathbf{r}'|} d\mathbf{r}' + \frac{\delta E_{xc}^{LSD}[\bar{n}_\alpha(\mathbf{r})]}{\delta n_\alpha(\mathbf{r})} - \beta \sigma \cdot \frac{\delta E_{xc}^{LSD}[\bar{n}_\alpha(\mathbf{r})]}{\delta m_\alpha(\mathbf{r})} \right) \quad (15)$$

The task of finding the single particle-like wavefunctions is now considerably more challenging than for the bare LSD because every state experiences a different potential. To maintain the orthogonality of the $\psi_\alpha(\mathbf{r})$ it is necessary to calculate the Lagrange multiplier matrix, $\lambda_{\alpha\alpha'}$.

As written in Eqs. (10-13), $E^{SIC-LSD}$ appears to be a functional of the set of occupied orbitals rather than of the total spin density only, like E^{LSD} . By a reformulation it may be shown^{25,26} that $E^{SIC-LSD}$ can in fact be regarded as a functional of the total spin density only. The associated exchange-correlation energy functional $E_{xc}^{SIC}[\bar{n}(\mathbf{r})]$ is, however, only implicitly defined,²⁶ for which reason the associated Kohn-Sham equations are rather impractical to exploit. For periodic solids the SIC-LSD approximation is a genuine extension of the LSD approximation in the sense that the self-interaction correction is only finite for localized states, which means that for Bloch-like single-particle states $E^{SIC-LSD}$ coincides with E^{LSD} . Therefore, the LSD minimum is also a local minimum of $E^{SIC-LSD}$. In

some cases another set of single-particle states may be found, not all being in Bloch form, to provide a local minimum for $E^{SIC-LSD}$. For this to happen some states must exist which can benefit from the self-interaction term without losing too much band formation energy. This usually will be the case for rather well localized states like the 3d states in transition metal oxides or the 4f states in rare earth compounds. Thus, $E^{SIC-LSD}$ is a single density functional, which may be used to describe localized as well as delocalized electron states.

We have solved the SIC-LSD equations self-consistently for a periodic solid using the unified Hamiltonian approach described by Temmerman et al.³⁷. The equations have been solved on a periodic lattice using the relativistic LMTO method in the tight-binding representation.

B. The Relativistic Spin-Polarised LMTO Method

In section C, $u_{\Lambda'}(\mathbf{r})$ with $\Lambda' = j, \mathbf{k}$ will be a general notation for the unoccupied intermediate states in the second order perturbation theory. For a crystalline material this is a Bloch state

$$u_{j\mathbf{k}}(\mathbf{r} + \mathbf{R}) = e^{i\mathbf{k}\cdot\mathbf{R}} u_{j\mathbf{k}}(\mathbf{r}), \quad (16)$$

where \mathbf{k} is the wavevector defined to be in the first Brillouin zone, and j is the band index. In the LMTO method the Bloch wave functions may be expanded in several ways²⁴. For the calculation of observables it is most convenient to make an expansion in terms of the single site solutions of the radial Dirac equation and their energy derivatives. For the relativistic spin-polarised case this has been achieved by Ebert^{38,39} and it is this method that we employ. The Bloch state is written as

$$u_{j\mathbf{k}}(\mathbf{r}) = \sum_{t=1}^{N_{\text{type}}} \sum_{i=1}^{N_t} \sum_{\Lambda} \left(A_{ti\Lambda}^{j\mathbf{k}} \phi_{\nu t\Lambda}(\mathbf{r} - \tau_i^t) + B_{ti\Lambda}^{j\mathbf{k}} \dot{\phi}_{\nu t\Lambda}(\mathbf{r} - \tau_i^t) \right) \quad (17)$$

Here

$$\phi_{\nu t\Lambda}(\mathbf{r}_t) = \sum_{\kappa'} \left(\begin{array}{l} g_{\kappa' \kappa}^{(t)m_j}(E_\nu, \mathbf{r}_t) \chi_{\kappa'}^{m_j}(\hat{\mathbf{r}}_t) \\ i f_{\kappa' \kappa}^{(t)m_j}(E_\nu, \mathbf{r}_t) \chi_{-\kappa'}^{m_j}(\hat{\mathbf{r}}_t) \end{array} \right) \quad (18)$$

and $\dot{\phi}_{\nu t\Lambda}(\mathbf{r}_t)$ is its energy derivative. These satisfy

$$\langle \phi_{\nu t\Lambda}(\mathbf{r}) | \phi_{\nu t\Lambda}(\mathbf{r}) \rangle = 1 \quad \langle \phi_{\nu t\Lambda}(\mathbf{r}) | \dot{\phi}_{\nu t\Lambda}(\mathbf{r}) \rangle = 0 \quad (19)$$

where the subscript ν corresponds to the energy E_ν about which the muffin tin orbitals of Eq. (18) are expanded. The single particle functions $\phi_{\nu t\Lambda}(\mathbf{r})$ and $\dot{\phi}_{\nu t\Lambda}(\mathbf{r})$ are evaluated at energy E_ν . In this relativistic formulation $\Lambda \equiv (\kappa, m_j)$ labels the boundary condition for the independent single-site solution $\phi_{\nu t\Lambda}(\mathbf{r} - \tau_i^t)$ of the Dirac equation about the site τ_i^t . N_{type} is the number of different types of atom in the unit cell. N_t is the number of equivalent atoms of type t . The coefficients $A_{ti\Lambda}^{j\mathbf{k}}$ and $B_{ti\Lambda}^{j\mathbf{k}}$ are written in terms of the LMTO structure constants and potential parameters, and are completely determined by a self-consistent LMTO calculation of the electronic structure²⁴. Key observables are then given in terms of these quantities. In particular the spin moment is

$$m_S = \sum_j \int_{E < E_f} m_s^{j\mathbf{k}} d\mathbf{k} \quad (20)$$

where

$$m_s^{j\mathbf{k}} = \sum_{t,i} \sum_{\Lambda} \sum_{\Lambda'} \left(\begin{array}{l} A_{ti\Lambda}^{j\mathbf{k}*} A_{ti\Lambda'}^{j\mathbf{k}} \langle \phi_{\nu t\Lambda}(\mathbf{r}_t) | \beta \sigma_z | \phi_{\nu t\Lambda'}(\mathbf{r}_t) \rangle + B_{ti\Lambda}^{j\mathbf{k}*} B_{ti\Lambda'}^{j\mathbf{k}} \langle \dot{\phi}_{\nu t\Lambda}(\mathbf{r}) | \beta \sigma_z | \dot{\phi}_{\nu t\Lambda'}(\mathbf{r}) \rangle \\ + A_{ti\Lambda}^{j\mathbf{k}*} B_{ti\Lambda'}^{j\mathbf{k}} \langle \phi_{\nu t\Lambda}(\mathbf{r}) | \beta \sigma_z | \dot{\phi}_{\nu t\Lambda'}(\mathbf{r}) \rangle + B_{ti\Lambda}^{j\mathbf{k}*} A_{ti\Lambda'}^{j\mathbf{k}} \langle \dot{\phi}_{\nu t\Lambda}(\mathbf{r}) | \beta \sigma_z | \phi_{\nu t\Lambda'}(\mathbf{r}) \rangle \end{array} \right) \quad (21)$$

and the orbital moment is

$$m_L = \sum_j \int_{E < E_f} m_l^{j\mathbf{k}} d\mathbf{k} \quad (22)$$

where

$$m_l^{j\mathbf{k}} = \sum_{t,i} \sum_{\Lambda} \sum_{\Lambda'} \left(\begin{array}{l} A_{ti\Lambda}^{j\mathbf{k}*} A_{ti\Lambda'}^{j\mathbf{k}} \langle \phi_{\nu t\Lambda}(\mathbf{r}_t) | \beta l_z | \phi_{\nu t\Lambda'}(\mathbf{r}_t) \rangle + B_{ti\Lambda}^{j\mathbf{k}*} B_{ti\Lambda'}^{j\mathbf{k}} \langle \dot{\phi}_{\nu t\Lambda}(\mathbf{r}) | \beta l_z | \dot{\phi}_{\nu t\Lambda'}(\mathbf{r}) \rangle \\ + A_{ti\Lambda}^{j\mathbf{k}*} B_{ti\Lambda'}^{j\mathbf{k}} \langle \phi_{\nu t\Lambda}(\mathbf{r}) | \beta l_z | \dot{\phi}_{\nu t\Lambda'}(\mathbf{r}) \rangle + B_{ti\Lambda}^{j\mathbf{k}*} A_{ti\Lambda'}^{j\mathbf{k}} \langle \dot{\phi}_{\nu t\Lambda}(\mathbf{r}) | \beta l_z | \phi_{\nu t\Lambda'}(\mathbf{r}) \rangle \end{array} \right) \quad (23)$$

C. The X-Ray Scattering Cross Section

In this section we will outline the formal first principles theory of magnetic x-ray scattering. It is based on the fully relativistic spin-polarised LMTO method in conjunction with 2nd order time-dependent perturbation theory. To simplify the presentation a straightforward canonical perturbation theory³⁶ is presented rather than a more sophisticated diagrammatic method⁴⁰.

1. Basic theory of x-ray scattering

The theory of x-ray scattering is based on the second order golden rule for the transition probability per unit time:

$$w_{if} = \frac{2\pi}{\hbar} \left| \langle f | \hat{H}'_{\text{int}} | i \rangle + \sum_I \frac{\langle f | \hat{H}'_{\text{int}} | I \rangle \langle I | \hat{H}'_{\text{int}} | i \rangle}{E_i - E_I} \right|^2 \delta(E_f - E_i) \quad (24)$$

where $|i\rangle$, $|I\rangle$ and $|f\rangle$ are the initial, intermediate and final states of the electron-photon system. E_i , E_I , and E_f are the corresponding energies. \hat{H}'_{int} is the time-independent part of the photon-electron interaction operator. The formalism to reduce this general expression to single-electron-like form has been published previously⁹. Therefore we will not repeat the details here, but only the equations that are key to the present implementation.

In relativistic quantum theory it is the second term in Eq. (24) that is entirely responsible for scattering as it is second order in the vector potential. It is convenient to divide this term into four components. To see this note that there are just two types of intermediate state $|I\rangle$, those containing no photons and those containing two photons. We can also divide up the scattering amplitude according to whether or not the intermediate states contain excitations from the ‘negative energy sea of electrons’, i.e. the creation of particle/antiparticle pairs. Therefore, if we assume elastic scattering, we can write

$$\begin{aligned} \sum_I \frac{\langle f | \hat{H}'_{\text{int}} | I \rangle \langle I | \hat{H}'_{\text{int}} | i \rangle}{E_i - E_I} &= f_{\mathbf{q}\lambda;\mathbf{q}'\lambda'}^{+\text{pos}}(\omega) + f_{\mathbf{q}\lambda;\mathbf{q}'\lambda'}^{-\text{pos}}(\omega) + f_{\mathbf{q}\lambda;\mathbf{q}'\lambda'}^{+\text{neg}}(\omega) + f_{\mathbf{q}\lambda;\mathbf{q}'\lambda'}^{-\text{neg}}(\omega) \\ &= \sum_{\Lambda\Lambda'} \frac{\int d\mathbf{r} u_{\Lambda}^{\dagger}(\mathbf{r}) X_{\mathbf{q}'\lambda'}^{\dagger}(\mathbf{r}) u_{\Lambda'}(\mathbf{r}) \int d\mathbf{r}' u_{\Lambda'}^{\dagger}(\mathbf{r}') X_{\mathbf{q}\lambda}(\mathbf{r}') u_{\Lambda}(\mathbf{r}')}{E_{\Lambda} - E_{\Lambda'} + \hbar\omega} \quad [1] \\ &+ \sum_{\Lambda\Lambda'} \frac{\int d\mathbf{r} u_{\Lambda}^{\dagger}(\mathbf{r}) X_{\mathbf{q}\lambda}(\mathbf{r}) u_{\Lambda'}(\mathbf{r}) \int d\mathbf{r}' u_{\Lambda'}^{\dagger}(\mathbf{r}') X_{\mathbf{q}'\lambda'}^{\dagger}(\mathbf{r}') u_{\Lambda}(\mathbf{r}')}{E_{\Lambda} - E_{\Lambda'} - \hbar\omega} \quad [2] \\ &+ \sum_{\Lambda\Lambda'} \frac{\int d\mathbf{r} v_{\Lambda}^{\dagger}(\mathbf{r}) X_{\mathbf{q}'\lambda'}^{\dagger}(\mathbf{r}) u_{\Lambda'}(\mathbf{r}) \int d\mathbf{r}' u_{\Lambda'}^{\dagger}(\mathbf{r}') X_{\mathbf{q}\lambda}(\mathbf{r}') v_{\Lambda}(\mathbf{r}')}{E_{\Lambda} - E_{\Lambda'} + \hbar\omega} \quad [3] \\ &+ \sum_{\Lambda\Lambda'} \frac{\int d\mathbf{r} v_{\Lambda}^{\dagger}(\mathbf{r}) X_{\mathbf{q}\lambda}(\mathbf{r}) u_{\Lambda'}(\mathbf{r}) \int d\mathbf{r}' u_{\Lambda'}^{\dagger}(\mathbf{r}') X_{\mathbf{q}'\lambda'}^{\dagger}(\mathbf{r}') v_{\Lambda}(\mathbf{r}')}{E_{\Lambda} - E_{\Lambda'} - \hbar\omega} \quad [4] \end{aligned} \quad (25)$$

The $f_{\mathbf{q}\lambda;\mathbf{q}'\lambda'}(\omega)$ are each termed scattering amplitudes. In Eq. (25) term [1] represents scattering with no photons and positive energy electrons only in the intermediate state, term [2] is when there are two photons and positive energy electrons only in the intermediate state, term [3] is for no photons and when negative energy electrons exist in the intermediate state and term [4] is for when two photons and negative energy electrons exist in the intermediate state. $u_{\Lambda}(\mathbf{r})$ and $v_{\Lambda}(\mathbf{r})$ are the positive and negative energy electron eigenstates of the Dirac Hamiltonian for the crystal. Λ, Λ' are labels for the one-electron states and, of course, are representation dependent. The positive energy one-electron states are subject to the constraint that $E_{\Lambda} \leq E_F$ and $E_{\Lambda'} > E_F$, where E_F is the Fermi energy. The relativistic electron-photon interaction vertex is

$$X_{\mathbf{q}\lambda}(\mathbf{r}) = -e \left(\frac{\hbar c^2}{2V\omega} \right)^{1/2} \boldsymbol{\alpha} \cdot \boldsymbol{\epsilon}^{(\lambda)} e^{i\mathbf{q} \cdot \mathbf{r}} \quad (26)$$

and \mathbf{q}, λ (\mathbf{q}', λ') represent the wavevector and polarisation of the incident (outgoing) photon. The $\boldsymbol{\alpha}$ ’s are the usual relativistic matrices in the standard representation and $\boldsymbol{\epsilon}^{(\lambda)}$ is the vector describing the polarisation of the photon. In Eq. (25) the last two terms are neglected. The justification for this is twofold. Firstly, in the energy range of interest

$\hbar\omega \ll 2mc^2$ these two terms have no resonance, and so will only make a contribution to the cross section that is slowly varying. This is to be compared with the resonant behaviour of the first term. Secondly, in Thomson scattering, where the negative energy states play a key role, all the electron states are extended. In a crystalline environment the negative energy states are largely extended while the states close to the Fermi energy are more localised, so one would expect the matrix elements to be smaller. Henceforth the first term in Eq. (25) will be referred to as the resonant term and the second as the non-resonant term.

In elastic scattering of x-rays $u_\Lambda(\mathbf{r})$ is an atomic-like core state localised at a lattice site. Although it is localised it is still an electron state of the crystal Hamiltonian. It is given by

$$u_{\Lambda_t}(\mathbf{r}_t) = \sum_{\kappa'} \begin{pmatrix} g_{\kappa'\kappa}^{(t)m_j}(\mathbf{r}_t) \chi_{\kappa'}^{m_j}(\hat{\mathbf{r}}_t) \\ i f_{\kappa'\kappa}^{(t)m_j}(\mathbf{r}_t) \chi_{-\kappa'}^{m_j}(\hat{\mathbf{r}}_t) \end{pmatrix} \quad (27)$$

where $g_{\kappa'\kappa}^{(t)m_j}(\mathbf{r})$ and $f_{\kappa'\kappa}^{(t)m_j}(\mathbf{r}_p)$ are solutions of the radial spin-polarised Dirac equation⁴¹ at the site t and $\chi_{\kappa'}^{m_j}(\hat{\mathbf{r}})$ are the usual spin-angular functions with spin-orbit quantum number κ ^{36,42}. As in Eq. (18) the sum over κ' runs over $\kappa' = \kappa$ and $\kappa' = -\kappa - 1$ only.

2. Evaluation of the Cross Section

The physical observable measured in MXRS experiments is the elastic differential cross section for scattering. This is given by

$$\frac{d\sigma}{d\Omega} = \frac{V^2}{4\pi^2} \frac{\omega^2}{\hbar^2 c^4} |f(\omega)|^2 \quad (28)$$

where the symbols have their usual meanings and we need to calculate the scattering amplitude $f(\omega)$ from Eq. (25). In this equation the integrals over \mathbf{r} and \mathbf{r}' extend over all space. However, the core states that appear in these integrals are well-localised on a particular site. Therefore it is an excellent approximation to limit the integrations to be within the same unit cell. This is also a good approximation from a physical viewpoint because in anomalous scattering of x-rays the core electron will be annihilated and created at the same atomic site. Then the scattering amplitudes become

$$\begin{aligned} f_{\mathbf{q}\lambda;\mathbf{q}'\lambda'}^{+\text{pos}}(\omega) &= \sum_N \sum_{j,\mathbf{k}} \sum_t \sum_{\Lambda_t} e^{-i(\mathbf{q}'-\mathbf{q}) \cdot \mathbf{R}_t} \frac{1}{E_{\Lambda_t} - E_{j\mathbf{k}} + \hbar\omega} \\ &\times \int d\mathbf{r}_t u_{\Lambda_t}^{t\dagger}(\mathbf{r}_t) X_{\mathbf{q}'\lambda'}^\dagger(\mathbf{r}_t) u_{j\mathbf{k}}(\mathbf{R}_t + \mathbf{r}_t) \int d\mathbf{r}'_t u_{j\mathbf{k}}(\mathbf{R}_t + \mathbf{r}'_t) X_{\mathbf{q}\lambda}(\mathbf{r}'_t) u_{\Lambda_t}(\mathbf{r}'_t) e^{-i(\mathbf{q}'-\mathbf{q}) \cdot \mathbf{R}_N} \end{aligned} \quad (29)$$

$$\begin{aligned} f_{\mathbf{q}\lambda;\mathbf{q}'\lambda'}^{-\text{pos}}(\omega) &= \sum_N \sum_{j,\mathbf{k}} \sum_t \sum_{\Lambda_t} e^{-i(\mathbf{q}'-\mathbf{q}) \cdot \tau_t} \frac{1}{E_{\Lambda_t} - E_{j\mathbf{k}} - \hbar\omega} \\ &\times \int d\mathbf{r}_t u_{\Lambda_t}^{t\dagger}(\mathbf{r}_t) X_{\mathbf{q}\lambda}(\mathbf{r}_t) u_{j\mathbf{k}}(\tau_t + \mathbf{r}_t) \int d\mathbf{r}'_t u_{j\mathbf{k}}^\dagger(\tau_t + \mathbf{r}'_t) X_{\mathbf{q}'\lambda'}^\dagger(\mathbf{r}'_t) u_{\Lambda_t}^t(\mathbf{r}'_t) e^{-i(\mathbf{q}'-\mathbf{q}) \cdot \mathbf{R}_N} \end{aligned} \quad (30)$$

where the sum over N is over unit cells. τ_t is the position of the t^{th} basis atom within the N^{th} unit cell and \mathbf{R}_N is a Bravais lattice vector. We may note several things about this expression to simplify it. Firstly, because we are assuming a perfect crystal the index N only necessarily appears in the final exponential. So

$$\sum_N e^{-i(\mathbf{q}'-\mathbf{q}) \cdot \mathbf{R}_N} = N_{\text{cells}} \delta_{\mathbf{q}'-\mathbf{q}, \mathbf{K}} \quad (31)$$

where N_{cells} is the number of unit cells in the crystal and \mathbf{K} is a reciprocal lattice vector. Secondly, Eqs. (29) and (30) contain a summation over \mathbf{k} -vectors. This can be transformed into a Brillouin zone integral :

$$\sum_{j\mathbf{k}} \rightarrow \sum_j \frac{V}{(2\pi)^3} \int_{\text{BZ}} d\mathbf{k} \quad (32)$$

where V is the crystal volume. Thirdly, the integrals over \mathbf{r}_t and \mathbf{r}'_t are single particle-like matrix elements and so a more concise notation can be used

$$m_{\Lambda_t}^{t,+,\mathbf{j}\mathbf{k}}(\mathbf{q}', \lambda') = \int d\mathbf{r}_t u_{\Lambda_t}^{t\dagger}(\mathbf{r}_t) X_{\mathbf{q}'\lambda'}^\dagger(\mathbf{r}_t) u_{j\mathbf{k}}(\tau_t + \mathbf{r}_t) \quad (33)$$

$$\begin{aligned} m_{j\mathbf{k}}^{t,-,\Lambda_t}(\mathbf{q}, \lambda) &= \int d\mathbf{r}'_t u_{j\mathbf{k}}(\tau_t + \mathbf{r}'_t) X_{\mathbf{q}\lambda}(\mathbf{r}'_t) u_{\Lambda_t}(\mathbf{r}'_t) \\ &= \left(\int d\mathbf{r}_t u_{\Lambda_t}^{t\dagger}(\mathbf{r}_t) X_{\mathbf{q}'\lambda'}^\dagger(\mathbf{r}_t) u_{j\mathbf{k}}(\tau_t + \mathbf{r}_t) \right)^* = m_{\Lambda_t}^{t,+,\mathbf{j}\mathbf{k}*}(\mathbf{q}', \lambda') \end{aligned} \quad (34)$$

$$m_{\Lambda_t}^{t,-,\mathbf{j}\mathbf{k}}(\mathbf{q}, \lambda) = \int d\mathbf{r}_t u_{\Lambda_t}^{t\dagger}(\mathbf{r}_t) X_{\mathbf{q},\lambda}(\mathbf{r}_t) u_{j\mathbf{k}}(\tau_t + \mathbf{r}_t) \quad (35)$$

$$\begin{aligned} m_{j\mathbf{k}}^{t,+,\Lambda_t}(\mathbf{q}', \lambda') &= \int d\mathbf{r}_t u_{j\mathbf{k}}^\dagger(\tau_t + \mathbf{r}_t) X_{\mathbf{q}'\lambda'}^\dagger(\mathbf{r}_t) u_{\Lambda_t}(\mathbf{r}_t) \\ &= \left(\int d\mathbf{r}_t u_{\Lambda_t}^{t\dagger}(\mathbf{r}_t) X_{\mathbf{q}'\lambda'}^\dagger(\mathbf{r}_t) u_{j\mathbf{k}}(\tau_t + \mathbf{r}_t) \right)^* = m_{\Lambda_t}^{t,-,\mathbf{j}\mathbf{k}*}(\mathbf{q}'\lambda') \end{aligned} \quad (36)$$

With these simplifications we can write the scattering amplitudes in a form familiar from Bragg diffraction theory

$$f_{\mathbf{q}\lambda;\mathbf{q}'\lambda'}^{+,\text{pos}}(\omega) = f_{0;\mathbf{q}\lambda;\mathbf{q}'\lambda'}^{+,\text{pos}}(\omega) N_{\text{cells}} \delta_{\mathbf{q}'-\mathbf{q},\mathbf{K}} \quad (37)$$

$$f_{\mathbf{q}\lambda;\mathbf{q}'\lambda'}^{-,\text{pos}}(\omega) = f_{0;\mathbf{q}\lambda;\mathbf{q}'\lambda'}^{-,\text{pos}}(\omega) N_{\text{cells}} \delta_{\mathbf{q}'-\mathbf{q},\mathbf{K}} \quad (38)$$

with a single unit cell contribution of

$$f_{0;\mathbf{q}\lambda;\mathbf{q}'\lambda'}^{+,\text{pos}}(\omega) = \sum_j^{E_j > E_f} \frac{V}{(2\pi)^3} \int_{\text{BZ}} d\mathbf{k} \sum_{t=1}^{N_{\text{type}}} \sum_{i=1}^{N_t} \sum_{\Lambda_t} e^{-i(\mathbf{q}'-\mathbf{q}) \cdot \tau_t} \frac{m_{\Lambda_t}^{t,+,\mathbf{j}\mathbf{k}}(\mathbf{q}', \lambda') m_{\Lambda_t}^{t,+,\mathbf{j}\mathbf{k}*}(\mathbf{q}, \lambda)}{E_{\Lambda_t} - E_{j\mathbf{k}} + \hbar\omega + i\Gamma/2} \quad (39)$$

$$f_{0;\mathbf{q}\lambda;\mathbf{q}'\lambda'}^{-,\text{pos}}(\omega) = \sum_j^{E_j > E_f} \frac{V}{(2\pi)^3} \int_{\text{BZ}} d\mathbf{k} \sum_{t=1}^{N_{\text{type}}} \sum_{i=1}^{N_t} \sum_{\Lambda_t} e^{-i(\mathbf{q}'-\mathbf{q}) \cdot \tau_t} \frac{m_{\Lambda_t}^{t,-,\mathbf{j}\mathbf{k}}(\mathbf{q}', \lambda') m_{\Lambda_t}^{t,-,\mathbf{j}\mathbf{k}*}(\mathbf{q}, \lambda)}{E_{\Lambda_t} - E_{j\mathbf{k}} - \hbar\omega + i\Gamma/2} \quad (40)$$

where we have introduced Γ , the natural width of the intermediate states, and which we treat as an adjustable parameter. These expressions are now in a form that is convenient for calculation from the output of an LMTO calculation.

3. Calculation of Matrix Elements

To perform the calculation of the transition rates and hence find the cross section for x-ray scattering we have to evaluate the matrix elements that appear in Eqs. (39) and (40) and that are defined by Eqs. (33) to (36). They can be calculated by substituting Eqs. (16), (17) and (27) into Eqs. (33) to (36). In the LMTO method the radial functions $\phi_{\nu t\Lambda}(\mathbf{r})$ are defined to be zero outside their atomic sphere²⁴. With a little manipulation the matrix elements can then be written

$$m_{\Lambda_t}^{ti,+,\mathbf{j}\mathbf{k}}(\mathbf{q}, \lambda) = \sum_{\Lambda} A_{ti\Lambda}^{j\mathbf{k}} \int d\mathbf{r}_i u_{\Lambda_t}^{t\dagger}(\mathbf{r}_i) X_{\mathbf{q}\lambda}^\dagger(\mathbf{r}_i) \phi_{\nu t\Lambda}(\mathbf{r}_i) + B_{ti\Lambda}^{j\mathbf{k}} \int d\mathbf{r}_i u_{\Lambda_t}^{t\dagger}(\mathbf{r}_i) X_{\mathbf{q}\lambda}^\dagger(\mathbf{r}_i) \dot{\phi}_{\nu t\Lambda}(\mathbf{r}_i) \quad (41)$$

$$m_{\Lambda_t}^{ti,-,\mathbf{j}\mathbf{k}}(\mathbf{q}, \lambda) = \sum_{\Lambda} A_{ti\Lambda}^{j\mathbf{k}} \int d\mathbf{r}_i u_{\Lambda_t}^{t\dagger}(\mathbf{r}_i) X_{\mathbf{q}\lambda}(\mathbf{r}_i) \phi_{\nu t\Lambda}(\mathbf{r}_i) + B_{ti\Lambda}^{j\mathbf{k}} \int d\mathbf{r}_i u_{\Lambda_t}^{t\dagger}(\mathbf{r}_i) X_{\mathbf{q}\lambda}(\mathbf{r}_i) \dot{\phi}_{\nu t\Lambda}(\mathbf{r}_i) \quad (42)$$

The individual matrix elements here are independent of position in the unit cell, and of the index i . They only depend on atom type. In these matrix elements the wavefunctions are four-component quantities and the operator $X_{\mathbf{q}\lambda}(\mathbf{r}_i)$ is a 4×4 quantity that contains the exponential

$$e^{i\mathbf{q} \cdot \mathbf{r}} \approx 1 + i\mathbf{q} \cdot \mathbf{r} + \dots \quad (43)$$

Retaining the first term in this expansion only corresponds to a dipole (E1) approximation. Including the second term corresponds to the electric quadrupole/magnetic dipole (E2/M1) approximation.

4. Matrix Elements in the E1 Approximation

If we insert Eqs. (17), (26) and (27) into the first integral in Eq. (41) with the dipole approximation we find the following expression

$$\begin{aligned} \int d\mathbf{r}_i u_{\Lambda_t}^{t\dagger}(\mathbf{r}_i) X_{\mathbf{q}\lambda}^\dagger(\mathbf{r}_i) \phi_{\nu t\Lambda}(\mathbf{r}_i) &\approx -iec \left(\frac{\hbar}{2V\epsilon_0\omega_q} \right)^{\frac{1}{2}} \sum_{\kappa'_t \kappa'} \left[\left(\int_0^{r_{WS}} dr r^2 g_{\kappa'_t \kappa_t}^{t, m_{jt}*}(r) f_{\kappa' \kappa}^{t, m_j}(E_\nu, r) \right) Q_{\kappa'_t, m_{jt}; -\kappa' m_j}^{-\lambda}(\mathbf{q}) \right. \\ &\quad \left. - \left(\int_0^{r_{WS}} dr r^2 f_{\kappa'_t \kappa_t}^{t, m_{jt}*}(r) g_{\kappa' \kappa}^{t, m_j}(E_\nu, r) \right) Q_{-\kappa'_t, m_{jt}; \kappa' m_j}^{-\lambda}(\mathbf{q}) \right] \end{aligned} \quad (44)$$

The second integral in Eq. (41) looks the same as this provided we make the replacements

$$g_{\kappa' \kappa}^{t, m_j}(E_\nu, r) \rightarrow \dot{g}_{\kappa' \kappa}^{t, m_j}(E_\nu, r) \quad (45)$$

$$f_{\kappa' \kappa}^{t, m_j}(E_\nu, r) \rightarrow \dot{f}_{\kappa' \kappa}^{t, m_j}(E_\nu, r) \quad (46)$$

and the angular integrals are defined by

$$Q_{\kappa, m_j; \kappa' m'_j}^\lambda(\mathbf{q}) = \int d\hat{\mathbf{r}} \chi_{\kappa}^{m_j\dagger}(\hat{\mathbf{r}}) \sigma \cdot \epsilon^\lambda(\mathbf{q}) \chi_{\kappa'}^{m'_j}(\hat{\mathbf{r}}) \quad (47)$$

where the σ are the usual 2×2 Pauli spin matrices and we have made use of the fact that $\epsilon^{\lambda*} = \epsilon^{-\lambda}$ for circularly polarised light. It is not necessary to calculate the dipole approximation to the integrals in Eq. (42) explicitly. They can be evaluated directly from Eq. (44). In the dipole approximation

$$X_{\mathbf{q}\lambda}(\mathbf{r}) = X_{\mathbf{q}-\lambda}^\dagger(\mathbf{r}) \quad (48)$$

we can see immediately that

$$ma_{\Lambda_t}^{ti, +, j\mathbf{k}}(\mathbf{q}, -\lambda) = ma_{\Lambda_t}^{ti, -, j\mathbf{k}}(\mathbf{q}, \lambda) \quad (49)$$

and we have written ma rather than m to indicate that these integrals are different from those in previous sections because they only include the first term in Eq. (43).

If the photon propagates along the direction of magnetisation (the z -axis) then the unit polarisation vectors for left (LCP) and right (RCP) circularly polarised light are $\epsilon^+(\mathbf{z}) = (1, i, 0)/\sqrt{2}$ and $\epsilon^-(\mathbf{z}) = (1, -i, 0)/\sqrt{2}$ respectively. To obtain the polarisation vectors for propagation directions away from the z -axis rotation matrices are applied to these vectors. Using the well-known orthonormality properties of the spherical harmonics the angular integrals in Eq. (47) yield

$$\begin{aligned} Q_{\kappa, m_j; \kappa' m'_j}^\lambda(\mathbf{q}) &= f_{11}(\theta_q, \phi_q, \lambda) C(l \frac{1}{2} j; m_j - \frac{1}{2}, \frac{1}{2}) C(l' \frac{1}{2} j'; m'_j - \frac{1}{2}, \frac{1}{2}) \delta_{ll'} \delta_{m_j, m'_j} \\ &\quad + f_{12}(\theta_q, \phi_q, \lambda) C(l \frac{1}{2} j; m_j - \frac{1}{2}, \frac{1}{2}) C(l' \frac{1}{2} j'; m'_j + \frac{1}{2}, -\frac{1}{2}) \delta_{ll'} \delta_{m_j, m'_j+1} \\ &\quad + f_{21}(\theta_q, \phi_q, \lambda) C(l \frac{1}{2} j; m_j + \frac{1}{2}, -\frac{1}{2}) C(l' \frac{1}{2} j'; m'_j - \frac{1}{2}, \frac{1}{2}) \delta_{ll'} \delta_{m_j, m'_j-1} \\ &\quad + f_{22}(\theta_q, \phi_q, \lambda) C(l \frac{1}{2} j; m_j + \frac{1}{2}, -\frac{1}{2}) C(l' \frac{1}{2} j'; m'_j + \frac{1}{2}, -\frac{1}{2}) \delta_{ll'} \delta_{m_j, m'_j} \end{aligned} \quad (50)$$

The angular factors $f_{ij}(\theta, \phi, \lambda)$ are determined by the photon polarisation and the direction of propagation. They are discussed in detail by Arola *et al.*⁹ The angular matrix elements of Eq. (47) determine the selection rules in the electric dipole approximation. They yield $l - l' = \pm 1$ for RCP and LCP regardless of the propagation direction. They also give $m_j - m'_j = 0, \pm 1$, depending on propagation direction and polarisation state. We also note that the selection rules are different in the resonant and the non-resonant terms in the scattering amplitude because one contains λ and the other contains $-\lambda$. This fact can be exploited in the design of experiments.

5. Matrix Elements in the E2/M1 Approximation

In Eq. (43) the $i\mathbf{q},\mathbf{r}$ term is responsible for the E2/M1 corrections to the electric dipole approximation. To calculate this correction we have to evaluate a new set of matrix elements which we denote $mb_{\Lambda_t}^{ti,+,\mathbf{j}\mathbf{k}}(\mathbf{q}, -\lambda)$ and $mb_{\Lambda_t}^{ti,-,\mathbf{j}\mathbf{k}}(\mathbf{q}, -\lambda)$ where the label b indicates that this is the correction to the dipole term. If we take the first term in Eq. (41) to this level of approximation we have

$$\begin{aligned} \int d\mathbf{r}_i u_{\Lambda_t}^{t\dagger}(\mathbf{r}_i) X b_{\mathbf{q}\lambda}^{\dagger}(\mathbf{r}_i) \phi_{\nu t\Lambda}(\mathbf{r}_i) &= -ec\mathbf{q} \left(\frac{\hbar}{2V\epsilon_0\omega} \right)^{\frac{1}{2}} \sum_{\kappa'_t \kappa'} \left[\left(\int_0^{r_{WS}} dr r^3 g_{\kappa'_t \kappa_t}^{t, m_{jt}*}(r) f_{\kappa' \kappa}^{t, m_j}(E_\nu, r) \right) P_{\kappa'_t, m_{jt}; -\kappa' m_j}^{-\lambda}(\mathbf{q}) \right. \\ &\quad \left. - \left(\int_0^{r_{WS}} dr r^3 f_{\kappa'_t \kappa_t}^{t, m_{jt}*}(r) g_{\kappa' \kappa}^{t, m_j}(E_\nu, r) \right) P_{-\kappa'_t, m_{jt}; \kappa' m_j}^{-\lambda}(\mathbf{q}) \right] \end{aligned} \quad (51)$$

To obtain the second integral in Eq. (41) we only have to make the substitutions (45) and (46) again. We now have a different set of angular integrals

$$P_{\kappa, m_j; \kappa' m'_j}^{\lambda}(\mathbf{q}) = \int d\hat{\mathbf{r}} \chi_{\kappa}^{m_j\dagger}(\hat{\mathbf{r}}) \sigma \cdot \epsilon^{\lambda}(\mathbf{q}) \hat{\mathbf{q}} \cdot \hat{\mathbf{r}} \chi_{\kappa'}^{m'_j}(\hat{\mathbf{r}}) \quad (52)$$

A similar expression can be obtained for the non-resonant contributions to the scattering amplitude if we make the replacement

$$P_{\kappa, m_j; \kappa' m'_j}^{-\lambda}(\mathbf{q}) \rightarrow -P_{\kappa, m_j; \kappa' m'_j}^{\lambda}(\mathbf{q}) \quad (53)$$

and so

$$mb_{\Lambda_t}^{ti,-,\mathbf{j}\mathbf{k}}(\mathbf{q}, \lambda) = -mb_{\Lambda_t}^{ti,+,\mathbf{j}\mathbf{k}}(\mathbf{q}, -\lambda) \quad (54)$$

The angular integrals necessary to determine $P_{\kappa, m_j; \kappa' m'_j}^{\lambda}(\mathbf{q})$ can be done analytically and a lengthy expression for them is given by Arola *et al.*⁹. They lead to the selection rules $l - l' = 0, \pm 1, \pm 2$ with the restriction that $s \rightarrow p$ and $p \rightarrow s$ are forbidden. For the z-component of total angular momentum the selection rules are $m_j - m'_j = 0, \pm 1, \pm 2$. Which of these possible selection rules dominates the transition depends on the photon polarisation and the direction of both the incident and outgoing photons as well as the magnitude of the radial matrix elements.

The full matrix elements for the calculation of the cross section are given by the sum of the E1 and E2/M1 contributions.

III. RESULTS

In this section we discuss a series of calculations to illustrate the relativistic MXRS theory we have developed within the SIC-LSD method for ordered magnetic crystals, and to demonstrate explicitly what information is contained in the x-ray scattering cross section. For this we have chosen to examine fcc praseodymium for a detailed analysis of the theory. The reasons for this choice are as follows: (i) Praseodymium contains two localized f -electrons. Therefore, it is the simplest f -electron material for which we can arbitrarily alter both the spin and orbital contributions to the magnetic moment by selectively choosing beforehand for which electrons we apply the SIC correction. (ii) Being fcc it has only one atom per primitive cell and is therefore computationally efficient to work with. While the fcc structure is not the observed ground state of Pr there are indications that an fcc form can be procured by quenching from 1300K⁴³. (iii) Using nonrelativistic SIC-LSD we have obtained good agreement with experiment for the total energy and equilibrium lattice constant of praseodymium. (iv) Preliminary calculations indicate that for the rare earth M_{IV} and M_{V} edges the MXRS spectra are, to first order, independent of crystal structure, so the results we obtain may be provisionally compared with experiment.

A. Ground State Properties

We have performed a self-consistent fully relativistic SIC-LSD calculation of the electronic structure of praseodymium at a series of lattice constants on the fcc structure and found a minimum in the total energy as shown in Fig. 1, where the results are presented in terms of the Wigner-Seitz radius. The ‘experimental’ value of the

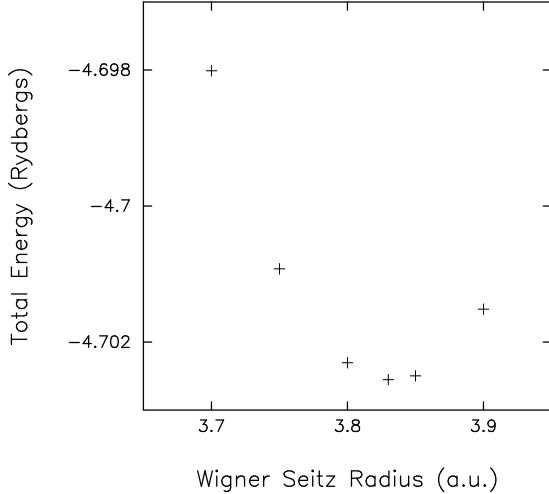


FIG. 1: The calculated SIC-LSD total energy of fcc praseodymium as a function of Wigner-Seitz radius. The electronic configuration corresponding to the Hund's rule ground state was used for these calculations. The theoretical prediction of the Wigner-Seitz radius is 3.82 a.u. Experimentally (see text) the value is 3.818 a.u.²⁴

TABLE I: This table displays the f-states selected for Self-Interaction correction and the self-consistently calculated spin and orbital magnetic moment of those states. The first column simply labels different configurations of localized states, the second column gives the m_l and m_s quantum numbers of the states from which self-interactions have been removed. Columns 3 and 4 are the calculated spin and orbital contribution to the total magnetic moment from the self-interaction corrected electrons and columns 5 and 6 are the calculated total spin and orbital contribution to the magnetic moment of fcc Pr. Note that the spin moment is fairly constant for all the selected configurations.

Configuration	$(m_l, m_s)_1$ $(m_l, m_s)_2$	$M_s(\text{SIC})$	$M_l(\text{SIC})$	$M_L(\text{tot})$	$M_S(\text{tot})$
1	(-3,1/2), (-2,1/2)	-4.96	+1.98	-4.79	2.42
2	(-3,1/2), (-1,1/2)	-3.95	+2.00	-3.91	2.43
3	(-3,1/2), (0,1/2)	-2.99	+1.99	-2.97	2.43
4	(-3,1/2), (1,1/2)	-1.96	+1.96	-1.97	2.48
5	(-3,1/2), (2,1/2)	-0.98	+1.99	-1.03	2.48
6	(-3,1/2), (3,1/2)	-0.005	+2.00	-0.05	2.52
7	(3,1/2), (-2,1/2)	1.00	+1.99	0.89	2.48
8	(3,1/2), (-1,1/2)	2.02	+1.97	1.84	2.50
9	(3,1/2), (0,1/2)	3.00	+1.98	2.75	2.49
10	(3,1/2), (1,1/2)	4.00	+1.97	3.80	2.52
11	(3,1/2), (2,1/2)	4.99	+1.99	4.69	2.54

Wigner-Seitz radius is determined as that which corresponds to the same volume per atom on the fcc lattice as is found in the naturally occurring DHCP crystal structure. Within the SIC-LSD method we can choose which electron states to correct for self-interaction. As the effect of the SIC is to localize the states this effectively determines which two of the 14 possible f states are occupied in trivalent praseodymium. All non-SI-corrected electrons are described using the standard Local Spin Density approximation via the unified Hamiltonian describing both localized and itinerant electrons. By trying all possible configurations and determining which arrangement of f electrons has the lowest total energy we can determine the ground state of praseodymium. In Table I we show a selection of possible states occupied by the two electrons with their self-consistently evaluated spin and orbital magnetic moments. In Fig. 2 we display the calculated total energy of these states against orbital moment. Note that we have chosen the spin moments parallel for all the states shown. For the antiparallel arrangement of electron spins the energy is significantly higher. It is clear that there is an approximately linear relationship between the total energy and orbital moment. For all the points on this figure the orbital as well as spin moments are computed self-consistently including the relaxation of the core states. The spin moments for all configurations of f electrons are found to be approximately the same, always being within 0.06 μ_B of 2.48 μ_B (See Table I). There is also a small increase in the magnitude of the (positive)

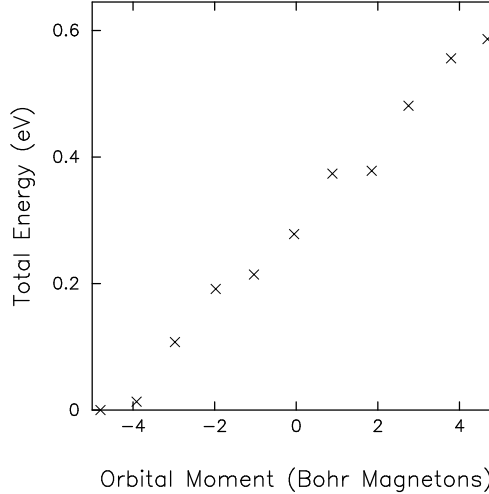


FIG. 2: The calculated total energy of fcc praseodymium as a function of orbital moment in Bohr magnetons for the states shown in table I. All magnetic moments were self-consistently determined and the spin moment was approximately constant for all the configurations shown. If an antiparallel arrangement of spins was selected the energies were considerably higher.

spin moment as the orbital moment increases from its most negative to its most positive values. This is due to the increasing effective field felt by the valence electrons. There is a slight variation in the spin moment values because the small hybridization of the non-SIC corrected f electrons with the $5d - 6s$ conduction band is dependent on the orbital character of the occupied states. Fig. 2 is consistent with the Hund's rules. The lowest energy state has f -spins parallel to each other in agreement with Hund's first rule. The total spin moment is $2.42\mu_B$ of which the two localized f electrons contribute $1.98\mu_B$, and the remainder comes from spin-polarization in the valence bands. The z component of the orbital magnetic moment is $-4.79\mu_B$ which is composed of $-4.97\mu_B$ from the localized f -electrons and $0.18\mu_B$ from the valence electrons. Note that the valence contribution to the orbital moment is parallel to the spin moment and antiparallel to the localized orbital moment. These numbers are fully consistent with Hund's second rule. Furthermore the f -shell is less than half full and the spin and orbital moments are found to be antiparallel in the lowest energy state, consistent with Hund's third rule. The fact that we can reproduce the expected lattice constant and f -electron configuration suggests very strongly that the electronic structure calculated using the relativistic SIC-LSD method describes the ground state properties of fcc praseodymium well. A detailed discussion of the electronic structure of the rare earth metals, calculated using the relativistic SIC-LSD method, will be published elsewhere⁴⁴

B. X-Ray Scattering Cross Sections

We have performed calculations of the x-ray scattering cross section at the M_{IV} and M_V absorption edges of Pr for all the f -electronic configurations shown in Table. I. These were evaluated with an arbitrary value of $\Gamma=1\text{eV}$ which is smaller than one would expect experimentally, but as the purpose of this section is to investigate the capability of the theory only rather than to make a strict comparison with experiment, it does not pose a problem. The effect of increasing Γ is simply to broaden and smooth out the calculated curve. A selection of the results is shown in Figs. 3 and 4. In each figure the cross section for left-handedly circularly polarized (LCP) photons, i.e. with positive helicity, and right-handedly circularly polarized (RCP) photons, i.e. with negative helicity, are shown. The geometrical setup of these calculations assumes that the propagation directions of the incident and outgoing photons are parallel to the exchange field, i.e. in our case parallel to the spin magnetic moment. Figures 3 and 4 show the cross section at the M_{IV} and M_V edges respectively as the SIC configuration is changed systematically such that the z component of the orbital moment varies from negative to positive values while at the same time the calculation shows that the spin moments remain nearly constant in magnitude and parallel to the exchange field. As the orbital moment increases we see that the cross section at the M_{IV} edge changes only slightly for LCP x-rays while for RCP x-rays it changes dramatically. At the most negative orbital moment the M_{IV} RCP cross section is very small, being completely overshadowed by the LCP peak. At the other end of the scale where the orbital moment is most positive the cross section for M_{IV} RCP x-rays is considerably larger than that for LCP x-rays. It should also be noted that the cross section peak for RCP x-rays is $1 - 2$ eV lower in energy than the peak for LCP x-rays.

When the resonant scattering ($E_{j\mathbf{k}} \approx E_{\Lambda_t} + \hbar\omega$) is close to the M_V edge, it is the RCP cross section that remains

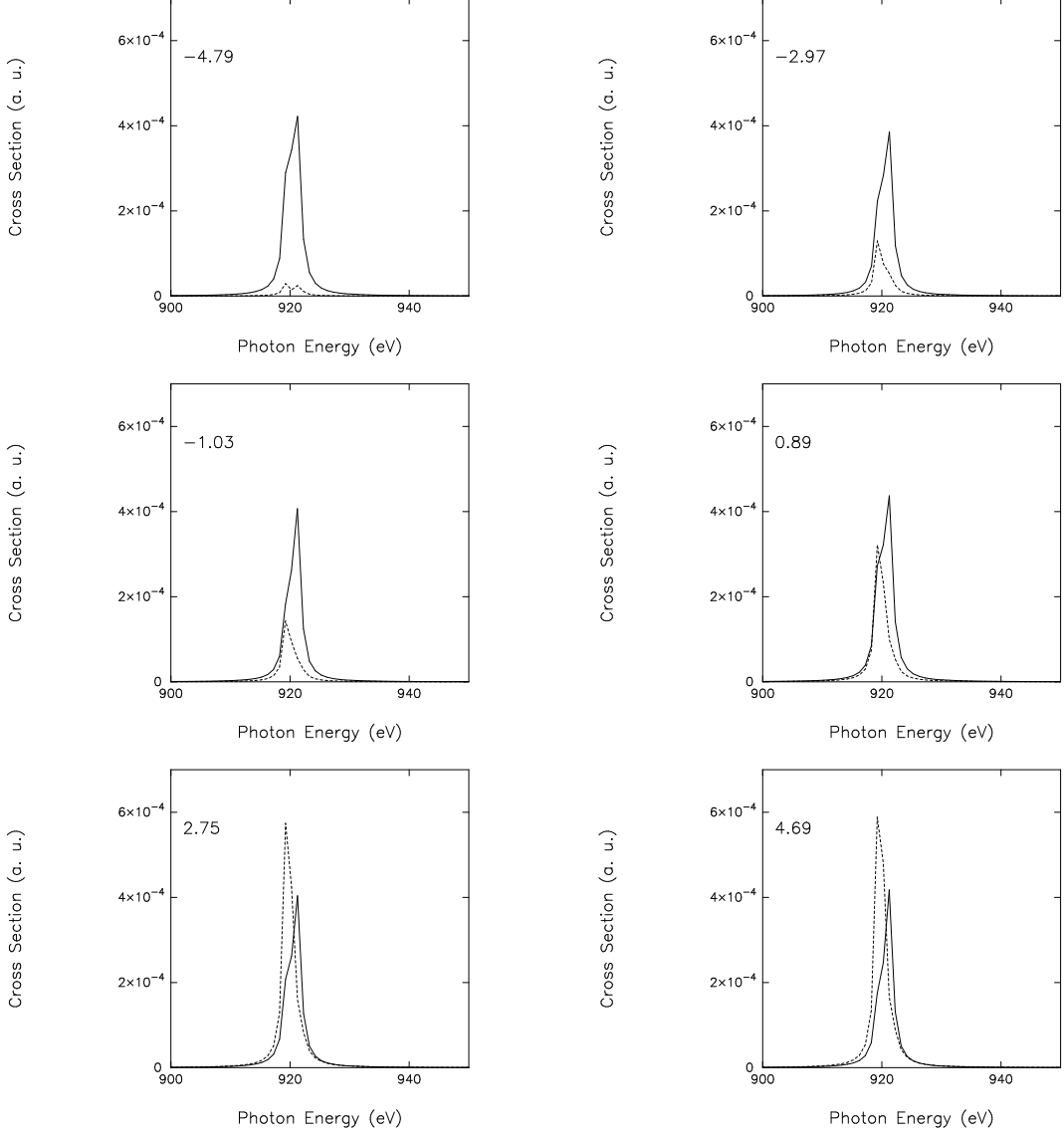


FIG. 3: The scattering cross section at the M_{IV} edge for praseodymium for electron configurations 1, 3, 5, 7, 9 and 11 from Table. I. Each figure is for a different pair of localized f -electrons. The calculated total orbital moment in Bohr magnetons is shown in the top left of each figure. The full curve is the cross section for x-rays with positive helicity and the dashed curve is that for negative helicity X-rays. A general trend of increasing magnitude of the cross section for negative helicity incident photons as the orbital moment increases from negative to positive is clearly observable in these curves. The positive helicity curve remains approximately constant with increasing orbital moment.

approximately constant with changing orbital moment, although a significant shoulder does appear on the low energy side of the curve as the orbital moment increases. The LCP peak decreases dramatically with increasing orbital moment. At the M_V edge, peaks from RCP and LCP x-ray scattering are again separated by 1 – 2 eV, but the ordering of the peaks is reversed from the case of the M_{IV} edge scattering.

Figures 3 and 4 indicate that the M_{IV} and M_V cross sections are directly related to the orbital moment of the constituent atoms, although they do not indicate the direct proportionality between magnetic moment and scattering cross section suggested by Blume¹. For example, the M_V edge cross section for LCP photons hardly varies in the upper two pictures in Fig. 4 despite a change of nearly $2\mu_B$ in the orbital moment. To clarify this point further, we show in Fig. 5 the cross section at the M_{IV} and M_V edges for SIC configurations that produce an orbital moment close to zero with the spins of the two occupied f states parallel. While neither the spin nor the orbital moment change significantly, the cross section certainly does. At the M_V edge the negative helicity curve is approximately constant while the positive helicity curve alters dramatically. On the other hand, at the M_{IV} edge it is the positive

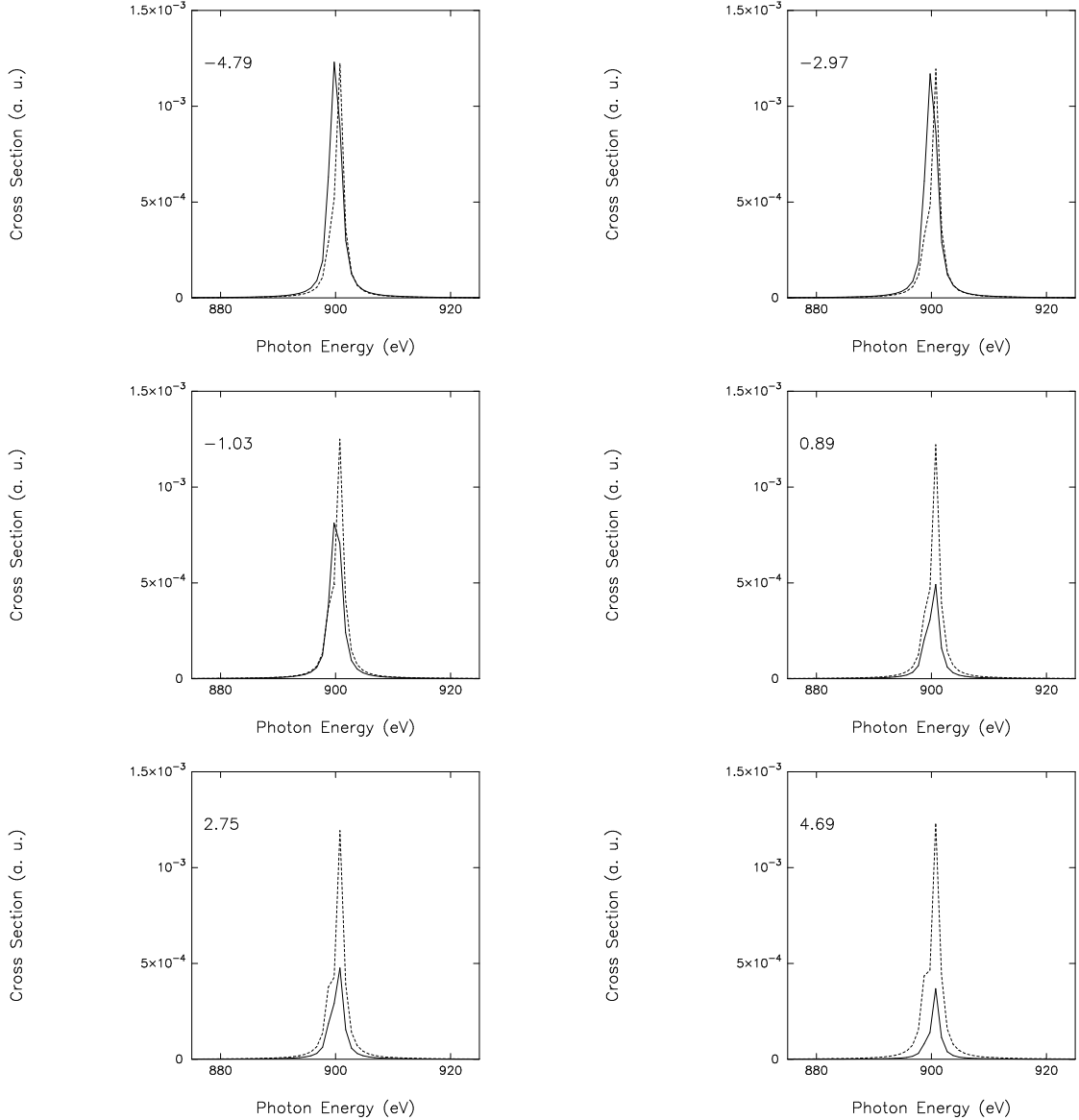


FIG. 4: The scattering cross section at the M_V edge for praseodymium for electron configurations 1, 3, 5, 7, 9 and 11 from Table I. Each figure is for a different pair of localized f -electrons. The calculated total orbital moment in Bohr magnetons is shown in the top left of each figure. The full curve is the cross section for x-rays with positive helicity and the dashed curve is that for negative helicity X-rays. A general trend of decreasing magnitude of the cross section for positive helicity incident photons with increasing orbital moment is clearly observable in these figures. The negative helicity curve remains fairly constant in magnitude with increasing orbital moment although the feature on the low energy side of the peak does become more pronounced.

helicity curve that is approximately constant while the negative one shows significant variation. This figure implies that the resonant x-ray scattering does not measure the total orbital moment, but is a measure of the orbital angular momentum of the individual one-electron states.

The important message of Figs. 3-5 is that the scattering cross section is not directly proportional to the total orbital moment of the material. However, both the spin and orbital moment have a strong influence on the size of the cross section peaks.

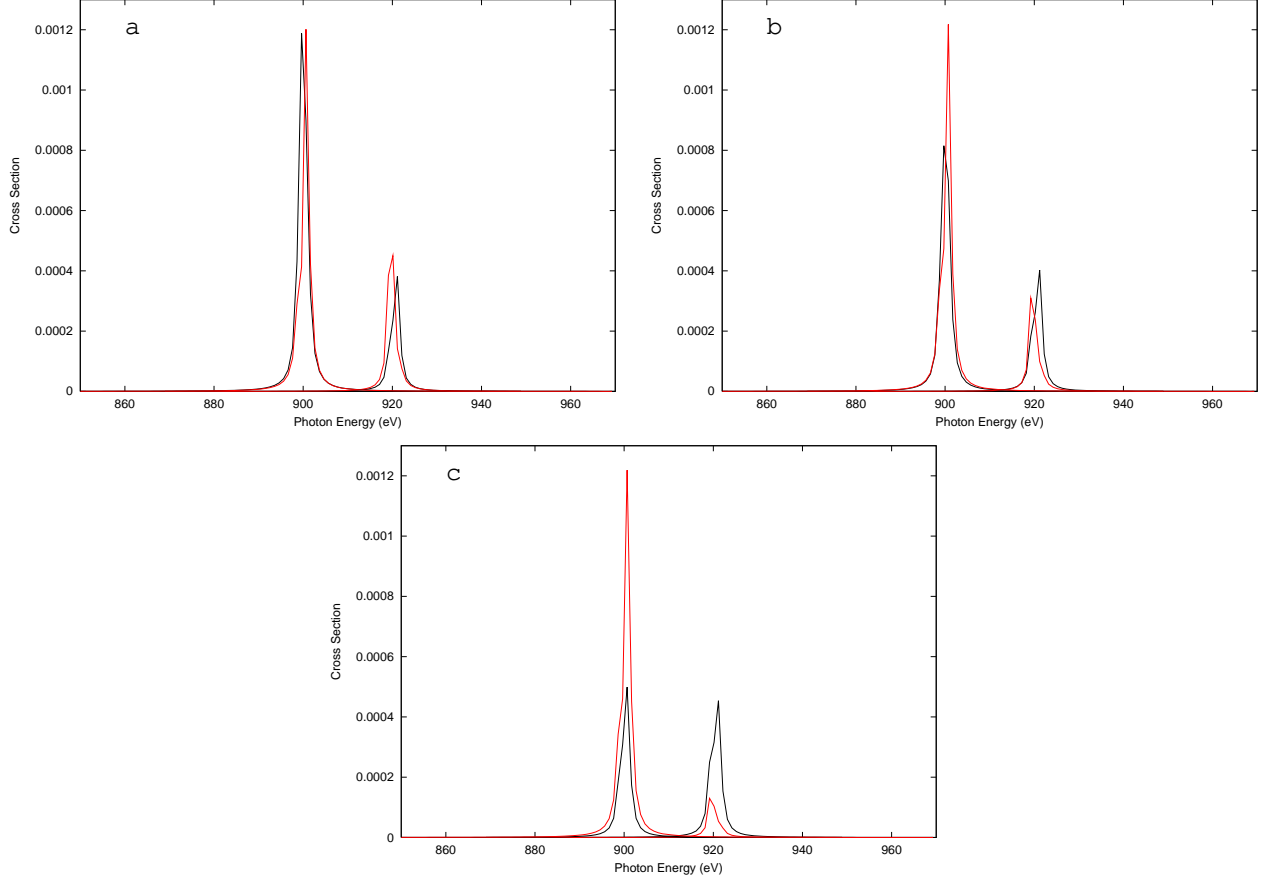


FIG. 5: The scattering cross section at the M_{IV} and M_{V} edges for praseodymium. Each figure is for a different SIC configuration but which produces roughly the same orbital and spin moment. The thick line is for negative helicity incident x-rays and the thin line is for positive helicity incident x-rays: (a) Localising the $m_l = -1$ and $m_l = +1$ electrons with spin up, yields an orbital moment of $-0.07\mu_B$ and a spin moment of $2.46\mu_B$; (b) Localising the $m_l = -2$ and $m_l = +2$ electrons with spin up, yields an orbital moment of $-0.12\mu_B$ and a spin moment of $2.47\mu_B$; (c) Localising the $m_l = -3$ and $m_l = +3$ electrons with spin up, yields an orbital moment of $-0.05\mu_B$ and a spin moment of $2.52\mu_B$.

IV. DISCUSSION

The standard theory of x-ray magnetic scattering is based on the work of Blume¹. He derived an equation for the nonresonant x-ray scattering cross section using a nonrelativistic approach with relativistic correction to order $1/c^2$. The resulting expression for the cross section, using his notation, is

$$\left(\frac{d^2\sigma}{d\Omega' dE'} \right)_{a \rightarrow b} = \left(\frac{e^2}{mc^2} \right)^2 \delta(E_a - E_b + \hbar\omega_k - \hbar\omega_{k'}) \times \left| \langle b | \sum_j e^{i\mathbf{K} \cdot \mathbf{r}_j} | a \rangle \epsilon' \cdot \epsilon - i \frac{\hbar\omega}{mc^2} \langle b | \sum_j e^{i\mathbf{K} \cdot \mathbf{r}_j} \left(i \frac{\mathbf{K} \times \mathbf{P}_j}{\hbar k^2} \cdot \mathbf{A} + \frac{\mathbf{s}_j \cdot \mathbf{B}}{\hbar} \right) | a \rangle \right|^2, \quad (55)$$

where E_a and E_b are the energies of the initial and final many-electron states, $|a\rangle$ and $|b\rangle$, respectively. $\mathbf{K} \equiv \mathbf{k} - \mathbf{k}'$, where \mathbf{k} and \mathbf{k}' are the wave vectors of the incoming and scattered photons, respectively, and \mathbf{r}_j , \mathbf{P}_j , and \mathbf{s}_j are electron (rigorously density functional state) coordinate, momentum, and spin operators.

$$\mathbf{A} \equiv \epsilon' \times \epsilon \quad (56)$$

and

$$\mathbf{B} \equiv \epsilon' \times \epsilon - (\hat{\mathbf{k}}' \times \epsilon') \times (\hat{\mathbf{k}} \times \epsilon) - (\hat{\mathbf{k}} \times \epsilon)(\epsilon' \cdot \hat{\mathbf{k}}) + (\hat{\mathbf{k}}' \times \epsilon')(\epsilon \cdot \hat{\mathbf{k}}') \quad (57)$$

depend only on the direction and polarization of the incident and emitted photons. The first term in Eq. (55) is the Thomson term, responsible for the charge scattering. The term containing \mathbf{A} depends on the orbital momentum and the term containing \mathbf{B} depends on the electron spin. This expression clearly shows that there are three distinct contributions to the magnetic scattering cross section, one from the orbital moment, the second from the spin moment, and the third from the interference term between the spin- and orbital moment. We also note the obvious point that if the orbital and spin moments of the individual electrons sum to zero, then the magnetic scattering vanishes. Most interestingly, Eq. (55) implies that, with a suitable choice of the photon energy, geometry and photon polarization it is possible to separate contributions to the cross section from the orbital and spin moments. However, this expression is not directly applicable in our resonant magnetic scattering studies because its derivation involves an approximation which is strictly not valid close to the resonance, while our approach is only valid around resonance because we ignore the negative energy contribution to the scattering amplitude, i.e. the terms that involve creation of virtual electron-positron pairs in the intermediate states in the second order perturbation theory (see Sec. II C of Ref. 9). Another difference from Blume's theory is the fact that our work is based on fully relativistic quantum mechanics, while Eq. (55) exploits the semi-relativistic approximation. This difference makes direct comparison of the two theories difficult. This has been discussed by Strange³⁶ who has rederived Eq. (55) as the nonrelativistic limit of a fully relativistic theory of x-ray scattering. For these reasons and the fact that there is no one-to-one correspondence between the terms in our expression for the scattering amplitude and Blume's expression, there is no straightforward way to compare the two theories. It is often stated that Blume's expression Eq. (55) shows that the cross section for magnetic scattering will yield the orbital and spin moment of a material separately. Although this will usually be the case it is not rigorously true. Eq. (55) cannot be applied immediately because the initial and final states $|a\rangle$ and $|b\rangle$ are general many-body states that have not been defined in detail. For implementation purposes they must be described as many-electron states that will contain the index j which is being summed over in Eq. (55). In a magnetic material the radial part of the basis functions of the single particle wavefunctions, as well as the angular part, depend on m_l . So, we would expect the total scattering amplitude to have a contribution from the orbital angular momentum associated with each single-particle state, but this is not the same as being proportional to the total orbital angular momentum. For example a two-particle state composed of two single-particle states with $m_l = \pm 1$ has the same z-component of orbital angular momentum as a two-particle state composed of two single-particle states with $m_l = \pm 3$, but Eq. (55) does not suggest that they will have the same scattering amplitude. Nonetheless, Blume's expression implies that a strong dependence of the cross section on the components of the magnetic moment is likely and indeed, this is exactly what we have found, an approximate, but by no means rigorous proportionality between orbital moment and magnitude of the cross section which is dependent on the polarization of the x-ray. Furthermore, figure 5 demonstrates explicitly the dependence of the cross section on the magnitude of m_l of the occupied individual electron states.

The question that now arises is how our computed x-ray scattering results can be interpreted in terms of the detailed electronic structure of praseodymium. In order to understand this we analyze the electronic structure of fcc Pr for the cases where the orbital moment is equal to $-4.79 \mu_B$, $-0.05 \mu_B$, and $4.69 \mu_B$ in detail. We expect the scattering cross section to reflect the Pr f -electron density of states. Although the shape of the cross section is partially determined by the density of states (DOS) the total DOS changes very little when pairs of electrons with differing orbital moments are localized. Therefore, a simple interpretation of the changes in the cross section with the orbital moment in terms of the total DOS cannot be made. In relativistic theories of magnetism different values of total angular momentum j with the same z-component m_j are coupled and further decomposition has little meaning⁴¹. To facilitate understanding of the differences in the spectra as orbital moment varies we show a selection of density of states curves, decomposed by the azimuthal quantum number m_j in Figs. 6–8. There are several points that should be noted about these pictures.

The $m_j = \pm 7/2$ (these are pure $j = l + 1/2$ states) figures describe f electron states with a well-defined j value, while all the others show f states with two different values of j ($j = l + 1/2$ and $j = l - 1/2$). In all the pictures except $m_j = \pm 7/2$ there are two main peaks, however these two peaks do not necessarily have the same weight. The separation of the peaks represents the spin and spin-orbit splitting of the individual values of m_j . The splitting between the unoccupied f -states is around 0.1 Ry while the splitting between the occupied and unoccupied states is about 0.7 Ry. The smaller narrow peaks in some of these figures represent the hybridization of different f -states between themselves. Some of these densities of states are markedly broader than others and this is a reflection of the degree of hybridization with the conduction $s - d$ electrons.

In Fig. 6 we have chosen to apply the self-interaction corrections to the f -electrons which correspond to ($m_l = -3, m_s = +\frac{1}{2}$) and ($m_l = -2, m_s = +\frac{1}{2}$) (Configuration 1 in Table 1) in the nonrelativistic limit, and this is reflected in the density of states having a very large and narrow peak at around -0.7 Rydbergs for $m_j = -5/2$ and $-3/2$. There is nothing for these states to hybridize with so they are very tall and narrow atomic-like states. For $m_j = -5/2$ and $-3/2$ the density of states has a more band-like component corresponding to a single electronic state just above the Fermi energy. For most of the other values of m_j there is a density of states corresponding to two electron states close to E_f and for $m_j = 7/2$ the density of states close to E_f corresponds to a single pure $j = l + 1/2$ state.

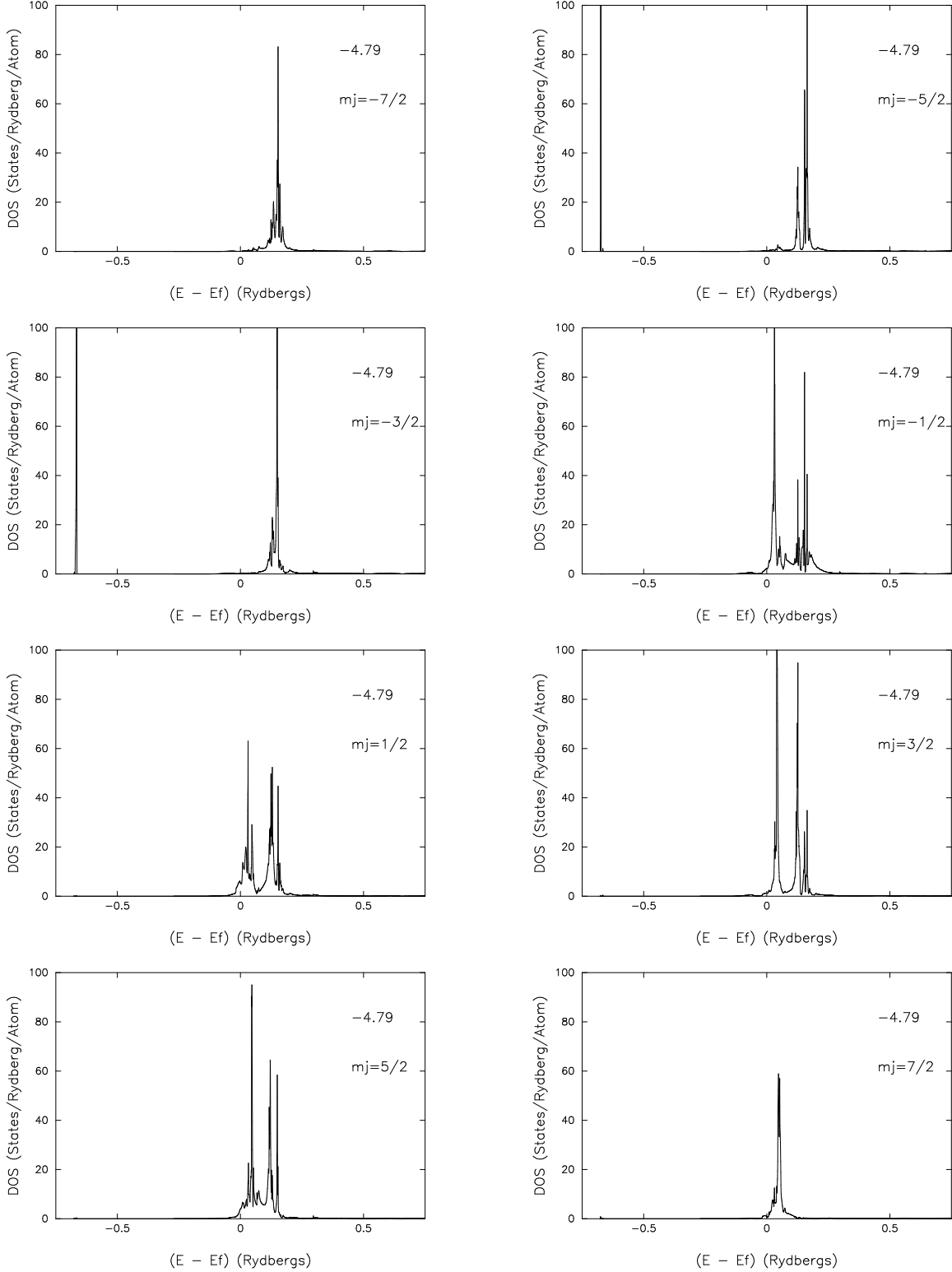


FIG. 6: The $l = 3$ contribution to the density of states of praseodymium decomposed by the m_j quantum number for the case when the $m_l = -3$ and $m_l = -2$ f states with spin up are occupied (localized). In the top right of each figure is the self-consistently calculated orbital moment. Each figure is also labelled with the relevant value of the m_j quantum number.

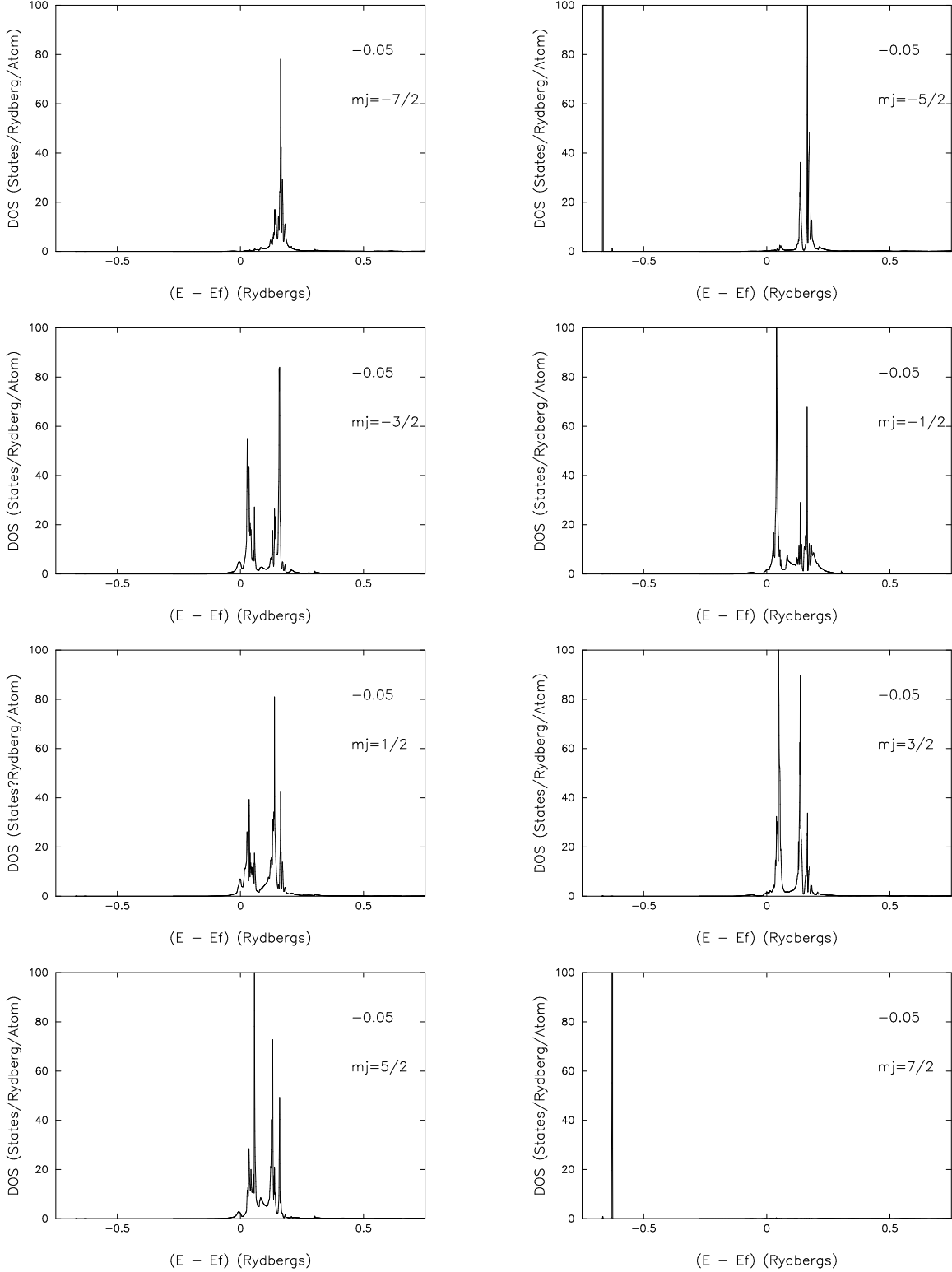


FIG. 7: The $l = 3$ contribution to the density of states of praseodymium decomposed by the m_j quantum number for the case when the $m_l = -3$ and $m_l = +3$ f states with spin up are occupied (localized). In the top right of each figure is the self-consistently calculated orbital moment. Each figure is also labelled with the relevant value of the m_j quantum number.

In Fig. 7 we have selected the f -electrons which correspond to $(m_l = -3, m_s = +\frac{1}{2})$ and $(m_l = +3, m_s = +\frac{1}{2})$ in the nonrelativistic limit for the SIC (Configuration 6 in Table 1). Here it is the $m_j = -5/2$ and the $m_j = +7/2$ components of the density of states that have the localized state around -0.7 Rydbergs below the Fermi energy. This means there is no $m_j = 7/2$ character around E_f at all in this case. For most other values of m_j we can clearly see that there are two f -states close to E_f . Detailed examination of these peaks shows that the dominant cause of the splitting is the exchange field, although the splitting is also influenced by the spin-orbit interaction. For $m_j = -7/2$ there is only one state close to E_f of course.

In Fig. 8 we have chosen to apply the self-interaction corrections to the f -electrons which correspond to $(m_l = +3, m_s = +\frac{1}{2})$ and $(m_l = +2, m_s = +\frac{1}{2})$ in the nonrelativistic limit (Configuration 11 in Table 1). This time it is the $m_j = 5/2$ and $m_j = 7/2$ states that are localized, and again there is no $m_j = 7/2$ character around E_f . The $m_j = -5/2$ and $m_j = -3/2$ state have the spin-split behaviour close to E_f in this case. The other values of m_j behave as before.

It is clear from figures 6 to 8 that in some m_j channels there is a small amount of band-like f -character below the Fermi energy. This indicates that there are two types of f -electron in our calculation, the localised f -electrons which determine the valence and the delocalised f -electrons which determine the valence transitions.¹⁶ It is the delocalised f -electrons that are principally responsible for the non-integer values of the orbital moments shown in figures 3 and 4, (although there is also a small contribution from the valence $s - d$ electrons).

Comparison of the corresponding diagrams in figures 6, 7 and 8 shows dramatic differences. Even though the total density of states is fairly insensitive to which f -electron states are occupied, the m_j -decomposed density of states is obviously drastically altered depending on which electrons are localized. In particular the f -states just above the Fermi energy form a significant number of the intermediate states in the formal theory described earlier. Therefore if key ones are localized they become unavailable as intermediate states for the spectroscopy and the cross section may be substantially altered. Of course, occupying one f -state means that some other f state is not occupied which may then also play a role as an intermediate state for the spectroscopy. Indeed, how much the unavailability of particular m_j substates affects the spectra depends on other factors too, including the E1 selection rules which are composed of angular matrix elements. Each angular matrix element contains four terms in the form of a product of Clebsch-Gordan coefficients and a geometry and polarization dependent factor (see Eqs. (23) and (24) of Ref. 9). A further influence is the fact that the LMTO coefficients A_{tiA}^{jk} (defined in Eq. (17) and completely determined by a self-consistent band structure calculation) associated with the f -electrons are found to be fairly independent of the rare earth element under consideration but their magnitude has a clear but complex linear proportionality to m_l .

Detailed analysis of the major contributions to the cross section suggests that the highest peak is formed by the core-to-valence transitions $(d_{\frac{5}{2}}, m_j) \rightarrow (f_{\frac{5}{2}}, m_j + (-)1)$ for the M_{IV} LCP(RCP) edge scattering and $(d_{\frac{5}{2}}, m_j) \rightarrow (f_{\frac{7}{2}}, m_j + (-)1)$ for the M_V LCP(RCP) edge scattering. The former transition for M_{IV} case is in agreement with the nonrelativistic selection rule which forbids a $\Delta j = 2$ transition, although this transition is not totally forbidden in the relativistic E1 selection rule. In the M_V case, the $\Delta j = 0$ transition is observed to form part of the shoulder rather than contributing to the main peak. Furthermore, within the transitions forming the main peak, the contribution to the LCP scattering at both the M_{IV} and M_V edge is the largest from the most positive allowed m_j value of the core state. On the other hand, the most negative m_j value of the core state gives the largest contribution to the RCP scattering. This indicates the fact that the Clebsch-Gordan coefficients which are used to calculate the selection rules are a dominant factor in determining the relative size of the cross section peaks.

From these considerations, we see that the separation of the LCP and RCP peaks by 1 to 2 electronvolts is a reflection of the spin-splitting of the states. In relativistic theory m_s and m_l are not good quantum numbers. Furthermore, because of the magnetism, different values of j with the same m_j are also coupled. However, it is still possible to associate $\langle s_z \rangle$, $\langle l_z \rangle$ with these quantum numbers and also to recognize the dominant j in atomic-like unhybridized bands. For example, in the case of LCP scattering at the M_{IV} edge, the largest contribution to the cross section comes from $(\kappa = 3, m_j = +\frac{5}{2})$ -like orbitals. The two $4f$ states which have this m_j as the main contributor are characterized by $(\langle s_z \rangle \simeq +\frac{1}{2}, \langle l_z \rangle \simeq +2)$ and $(\langle s_z \rangle \simeq -\frac{1}{2}, \langle l_z \rangle \simeq +3)$. Electronic structure calculation shows that the former state is dominated by $\kappa = -4$ and the latter by $\kappa = 3$. Therefore the M_{IV} LCP peak is most affected by the availability of the spin-down $\langle l_z \rangle \simeq 3$ state as an intermediate state. Similar analysis shows that the M_{IV} RCP peak is most affected by spin-up $\langle l_z \rangle \simeq -3$ state, M_V LCP by spin-up $\langle l_z \rangle \simeq 3$, and M_V RCP by spin-down $\langle l_z \rangle \simeq -3$ state.

Although this analysis is a gross simplification, it does explain why the relative peak energy positions in the LCP and RCP scattering cases swap between the M_{IV} and M_V edges (see Fig. 5). Of course this is true only if these states are still available after the chosen localizations by SIC. The effect of localization on the MXRS spectrum is most dramatic if SIC is applied to these key states, changing the peak energy separation as well as the scattering amplitude between the LCP and RCP scattering cases.

Some empty valence band f states participating in the scattering process have nearly equal mixture of the two j characters, i.e. $j = l + 1/2$ and $j = l - 1/2$. If there is strong spin-up and spin-down character in the unoccupied

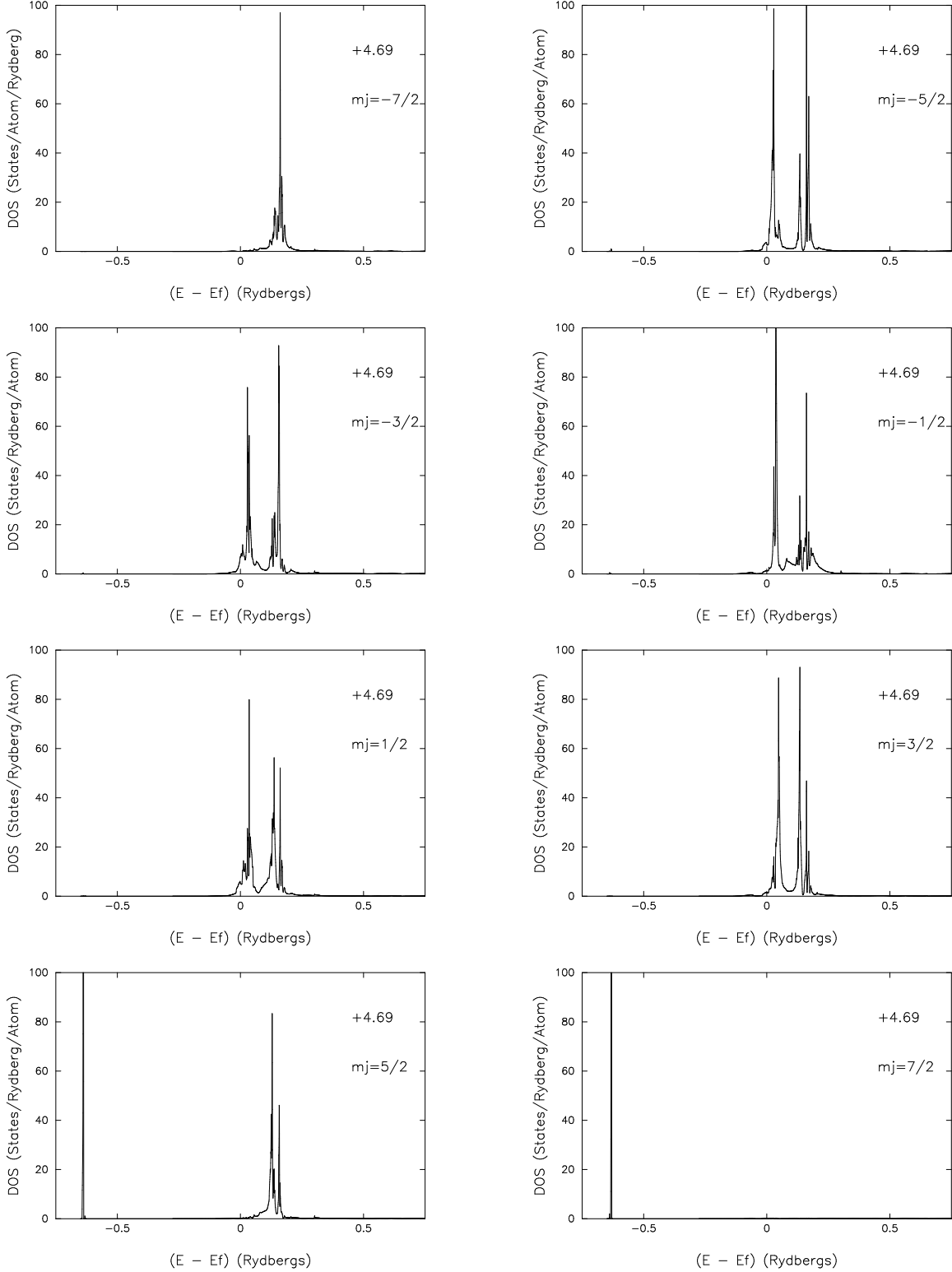


FIG. 8: The $l = 3$ contribution to the density of states of praseodymium decomposed by the m_j quantum number for the case when the $m_l = +3$ and $m_l = +2$ f states with spin up are occupied (localized). In the top right of each figure is the self-consistently calculated orbital moment. Each figure is also labelled with the relevant value of the m_j quantum number.

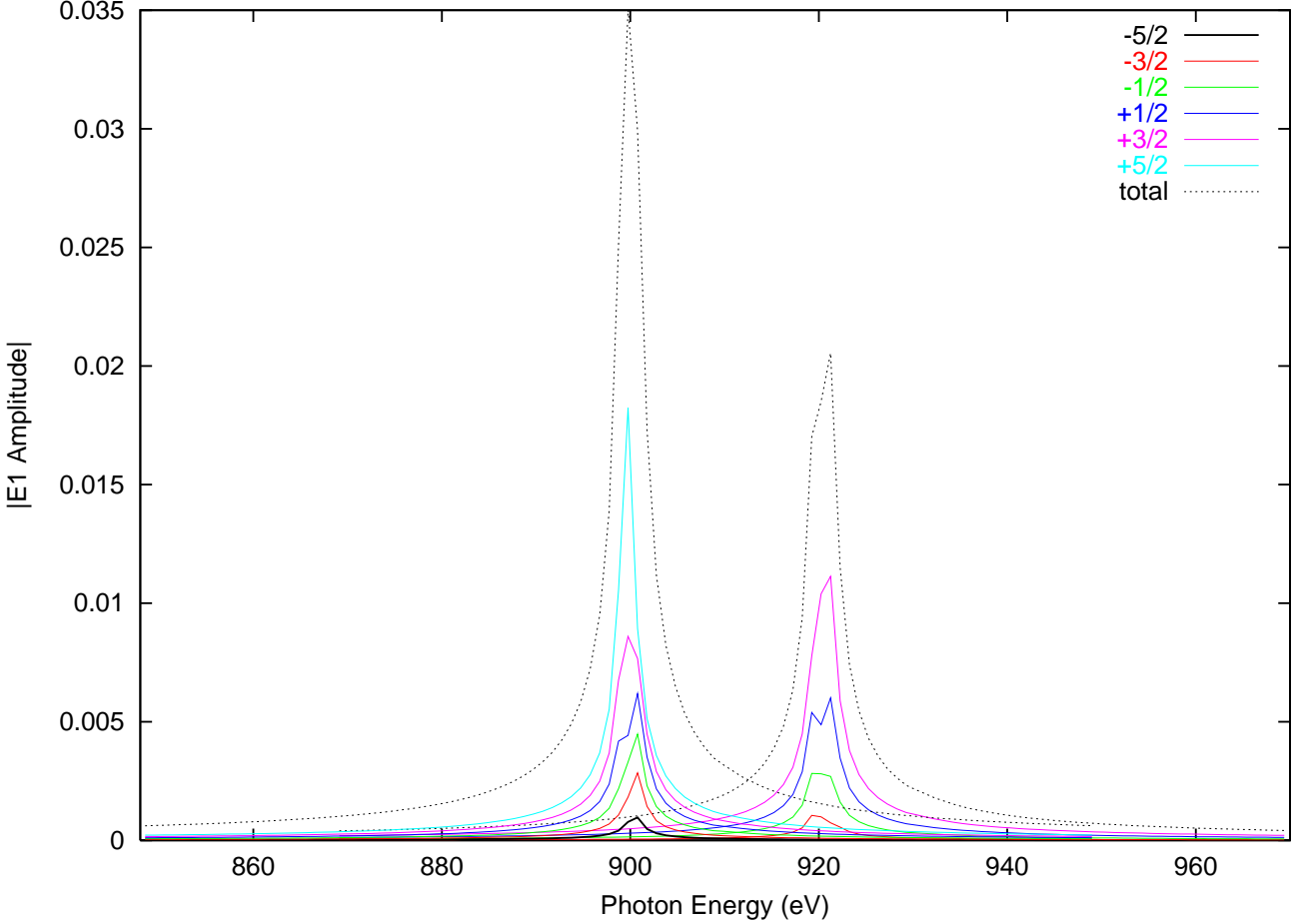


FIG. 9: Core m_j decomposed LCP amplitude at the M_{IV} and M_V edges. This figure is for the case when the $m_l = -3$ and $m_l = -2$ states are occupied.

valence states described by a specific m_j then both spin states may be available as the intermediate states for the spectroscopy. Thus we may clearly see a two-peak structure in the m_j decomposed amplitude for a certain polarization at the absorption edge. Figure 9 shows the core m_j decomposed LCP scattering amplitude and the two-peak structure mentioned above is clearly visible for $m_j = +\frac{1}{2}$ at the M_{IV} edge.

In certain cases we can interpret the apparent relation between the magnetic cross section and the z-component of the total orbital moment as follows. Because $\langle l_z \rangle + \langle s_z \rangle = \langle j_z \rangle$ holds, then we see that if we apply self interaction corrections to states systematically according to Hund's rules, what is effectively done is to occupy the states in order of m_j . As stated earlier the m_j decomposed relativistic magnetic scattering cross section has a 'proportionality' to m_j due to the Clebsch-Gordan coefficient in the angular matrix element expression defining the $E1$ selection rules. Whether this proportionality is direct or inverse depends on the polarization of x-rays. In addition, according to the electronic structure calculation, as the unhybridized state goes from $(\langle l_z \rangle \simeq -3, \langle s_z \rangle \simeq \frac{1}{2})$ to $(\langle l_z \rangle \simeq +3, \langle s_z \rangle \simeq \frac{1}{2})$, the dominant j changes from $j = \frac{5}{2}$ to $j = \frac{7}{2}$ gradually. This tells us two things. Firstly we notice that if a certain state has a major impact on the scattering cross section at the M_{IV} edge for RCP photons, then this same state has a relatively minor effect on the cross section for LCP photons at the same edge because of the Clebsch-Gordan factor in the expression for the $E1$ selection rules as mentioned above. Secondly we see that this same state also has only a minor effect on the M_V cross section because the value of j for the intermediate states involved in major transition differ between M_{IV} and M_V .

As the SIC configuration varies from $(\langle l_z \rangle \simeq -3, \langle s_z \rangle \simeq +\frac{1}{2})$ and $(\langle l_z \rangle \simeq -2, \langle s_z \rangle \simeq +\frac{1}{2})$ to $(\langle l_z \rangle \simeq -3, \langle s_z \rangle \simeq +\frac{1}{2})$ and $(\langle l_z \rangle \simeq +3, \langle s_z \rangle \simeq +\frac{1}{2})$ so that there is a systematic change in the z-component of the total orbital moment, the M_{IV} RCP cross section increases because the second, third and so on, strongest contributors to the cross section become additionally available as intermediate states as they are released from the SIC localization. However, they have progressively less impact as we proceed through this series of quantum numbers since the major j gradually changes to $j = \frac{7}{2}$. The cross section at the M_{IV} edge for LCP photons is not affected much by this change in quantum

numbers since neither the initial nor the final SIC combination in the above series involves the major contributors to M_{IV} LCP cross section. On the other hand, the M_V edge LCP cross section is reduced as more and more significant contributors are removed from the available intermediate states, while the cross section at the M_V edge for RCP photons is not much affected for the same reason as M_{IV} LCP case. Obviously the above change in SIC configuration is very artificial. However as the states are filled up according to Hund's rule as we proceed through the rare earth series, we would expect to observe changes in the cross section governed by these considerations for rare earths where the intermediate states can be considered as atomic-like. However, a very different interpretation of the x-ray spectra may be required in the case where delocalized band-like intermediate states are of primary importance, as is the case in resonant x-ray scattering at the K and $L_{II,III}$ edges.

Finally, we are unaware of any experimental measurements of the MXRS spectra of praseodymium or its compounds at the M_{IV} or M_V edge. However a careful combined neutron⁴⁵ and x-ray⁴⁶ (at the $L_{II,III}$ edges) investigation into the magnetism of Ho_xPr_{1-x} alloys has concluded that the Pr ion does have a 4f moment at all values of x . Deen *et al.*⁴⁷ have performed MXRS measurements at the L edges in Nd/Pr superlattices and found a large peak at the absorption edge and a high energy shoulder corresponding to dipolar transitions to the broad 5d band. We hope that our calculations will stimulate detailed experimental x-ray studies of M_{IV} and M_V edges of Pr, in pure Pr and in its alloys and compounds.

V. CONCLUSIONS

In conclusion, a theory of Magnetic X-Ray Scattering that is based on the LSD with self-interaction corrections and second order time-dependent perturbation theory has been described. We have illustrated the theory with an application to fcc Praseodymium and used this example to illustrate the dependence of the scattering cross section on spin and orbital magnetic moments. It has been shown that the theory quantitatively reproduces the dependence on the spin and orbital magnetic moments originally predicted qualitatively¹.

VI. ACKNOWLEDGEMENTS

MH would like to thank Keele University for a Ph.D studentship. PS and EA would like to thank the British EPSRC for grant number GR/M45399/01 during which the bulk of the work reported in this paper was carried out.

¹ M. Blume, *J. Appl. Phys.* **57**, 3615 (1985).
² M. Blume and D. Gibbs, *Phys. Rev. B* **37**, 1779 (1988).
³ J. P. Hannon, G. T. Trammell, M. Blume, and D. Gibbs, *Phys. Rev. Lett.* **61**, 1245 (1988).
⁴ A. Fasolino, P. Carra and M. Altarelli, *Phys. Rev. B* **47**, 3877 (1993).
⁵ P. Rennert, *Phys. Rev. B* **48**, 13 559 (1993).
⁶ S. W. Lovesey, K. S. Knight, and E. Balcar, *Phys. Rev. B* **64**, 054405 (2001); S. W. Lovesey, K. S. Knight, and D. S. Sivia, *Phys. Rev. B* **65**, 224402 (2002); S. W. Lovesey, *J. Phys. Condens. Matter* **14**, 4415 (2002).
⁷ P. Hohenberg and W. Kohn, *Phys. Rev.* **136**, B864 (1964); W. Kohn and L. J. Sham, *Phys. Rev. A* **140**, 1133 (1965).
⁸ W. Kohn and P. Vashishta, in *Theory of the Inhomogeneous Electron Gas*, edited by S. Lundqvist and N. H. March (Plenum Press, New York, 1982).
⁹ E. Arola, P. Strange and B. L. Gyorffy, *Phys. Rev. B* **55**, 472 (1997).
¹⁰ E. Arola and P. Strange, *Appl. Phys. A* **73**, 667 (2001).
¹¹ E. Arola, P. Strange, N. I. Kulikov, M. J. Woods, and B. L. Gyorffy, *J. Magn. Magn. Mater.* **177-181** 1415 (1998); E. Arola and P. Strange, *Phys. Rev. B* **58**, 7663 (1998).
¹² V. Anisimov, F. Aryasetiawan, and A. I. Lichtenstein, *J. Phys. Condens. Matter* **9**, 767 (1997).
¹³ Z. Szotek, W. M. Temmerman, and H. Winter, *Phys. Rev. B* **47**, 4029 (1993).
¹⁴ W. M. Temmerman, A. Svane, Z. Szotek and H. Winter, in *Electronic Density Functional Theory: Recent Progress and New Directions*, edited by J. F. Dobson, G. Vignale, and M. P. Das (Plenum, 1997).
¹⁵ A. Svane and O. Gunnarsson, *Phys. Rev. Lett.* **65**, 1148 (1990).
¹⁶ P. Strange, A. Svane, W. M. Temmerman, Z. Szotek, and H. Winter, *Nature* **399**, 756 (1999).
¹⁷ S. V. Beiden, W. M. Temmerman, Z. Szotek, and G. A. Gehring, *Phys. Rev. Lett.* **79**, 3970 (1997).
¹⁸ F. E. Low, *Phys. Rev.* **96**, 1428 (1954); M. Gell-Mann and M. L. Goldberger, *ibid.* **96**, 1433 (1954).
¹⁹ P. M. Platzman and N. Tzoar, *Phys. Rev. B* **2**, 3556 (1970).
²⁰ D. Gibbs, D. R. Harshman, E. D. Isaacs, D. B. McWhan, D. Mills, and C. Vettier, *Phys. Rev. Lett.* **61**, 1241 (1988).
²¹ The Xmas beamline at the European Synchrotron Radiation Facility, for example.

²² W. G. Stirling and M. J. Cooper, *J. Magn. Magn. Mater.* **200**, 755 (1999).

²³ M. J. Cooper and W. G. Stirling, *Radiation Physics and Chemistry* **56**, 85 (1999).

²⁴ O. K. Andersen and O. Jepsen, *Phys. Rev. Lett.* **53**, 2571 (1984); O. K. Andersen, O. Jepsen, and O. Glötzel, *Canonical Description of the Band Structures of Metals*, Proc. of Int. School of Physics, Course LXXXIX, Varenna, 1985, edited by F. Bassani, F. Fumi, and M. P. Tosi (North-Holland, Amsterdam, 1985), p. 59; H. L. Skriver, The LMTO Method, Springer series in Solid State Sciences Volume 41, Springer-Verlag, (1984); I. Turek, V. Drchal, J. Kudrnovsky, M. Sob, and P. Weinberger, *Electronic Structure of Disordered Alloys, Surfaces and Interfaces*, Kluwer Academic Publishers, (1997)

²⁵ J. P. Perdew and A. Zunger, *Phys. Rev. B* **23**, 5048 (1981).

²⁶ A. Svane, *Phys. Rev. B* **51**, 7924 (1995).

²⁷ Z. Szotek, W. M. Temmerman and H. Winter, *Phys. Rev. B* **47**, 4029 (1993).

²⁸ A. Svane and O. Gunnarsson, *Phys. Rev. B* **37**, 9919 (1988); A. Svane and O. Gunnarsson, *Europhys. Lett.* **7**, 171 (1988).

²⁹ J.A. Majewski and P. Vogl, *Phys. Rev. B* **46**, 12219 (1992); *ibid* **46**, 12235 (1992).

³⁰ A. Svane, *Phys. Rev. Lett.* **68**, 1900 (1992).

³¹ W.M. Temmerman, H. Winter, Z. Szotek and A. Svane, *Phys. Rev. Lett.* **86**, 2435, (2001).

³² W.M. Temmerman, Z. Szotek and H. Winter, *Phys. Rev. B* **47**, 1184, (1993)

³³ L. Petit, A. Svane, Z. Szotek and W.M. Temmerman, *Science*, **301**, 498, (2003)

³⁴ R. Tyer, W.M. Temmerman, Z. Szotek, G. Banach, A. Svane, L. Petit, and G.A. Gehring, *Europhys. Lett.* **65**, 519, (2004)

³⁵ A. Svane and O. Gunnarsson, *Solid State Commun.* **76**, 851 (1990).

³⁶ P. Strange, *Relativistic Quantum Mechanics, with applications in condensed matter and atomic physics*. Cambridge University Press (1998).

³⁷ W.M. Temmerman, A. Svane, Z. Szotek, H. Winter and S.V. Beiden, "On the implementation of the Self-Interaction Corrected Local Spin Density Approximation for *d*- and *f*-electron systems", Lecture notes in Physics 535: *Electronic Structure and Physical properties of Solids: The uses of the LMTO method* Edited by H. Dreysse, p286, (Springer-Verlag, Berlin, 2000).

³⁸ H. Ebert, *Phys. Rev. B* **38**, 9390, (1988).

³⁹ H. Ebert, P. Strange and B.L. Gyorffy, *J. Appl. Phys.* **63**, Part 2, 3052, (1988)

⁴⁰ P. J. Durham, in *Electronic Structure of Complex Systems*, edited by P. Phariseau and W. M. Temmerman, Vol. 113 of *NATO Advanced Study Institute, Series B: Physics* (Plenum Press, New York, 1984).

⁴¹ P. Strange, J.B. Staunton and B.L. Gyorffy, *J. Phys. C* **17**, 3355, (1984).

⁴² M. E. Rose, *Relativistic Electron Theory*, (John Wiley, New York) (1971).

⁴³ K. McEwen in *Handbook of the Physics and Chemistry of the Rare Earths*, Vol **1**, 411, (North Holland, 1978).

⁴⁴ P. Strange, M. Horne, Z. Szotek and P. Strange, in preparation.

⁴⁵ J.P. Goff, C. Bryn-Jacobsen, D.F. McMorrow, G.J. McIntyre, J.A. Simpson, R.C.C. Ward and M.R. Wells, *Phys. Rev. B*, **57**, 5933, (1998)

⁴⁶ A. Vigliante, M.J. Christensen, J.P. Hill, G. Helgesen, S.A. Sorensen, D.F. McMorrow, D. Gibbs, R.C.C. Ward and M.R. Wells, *Phys. Rev. B*, **57**, 5941, (1998).

⁴⁷ P.P. Deen, J.P. Goff, R.C.C. Ward, M.R. Wells and A. Stunault, *Journal of Magnetism and Magnetic Materials* **240**, 553, (2002).